Dendritic cell accumulation in the gut and central nervous system is differentially dependent on α4 integrins [1]

Christopher Sie [*, †], Laura Garcia Perez [‡], Mario Kreutzfeldt [§], Maria Potthast [¶], Caspar Ohnmacht [¶], Doron Merkler [§], Samuel Huber [‡], Anne Krug [‖], and Thomas Korn [*, †, #, 2]

[*] Department of Experimental Neuroimmunology, Klinikum rechts der Isar, Technical University of Munich, Munich, Germany

[†] Department of Neurology, Klinikum rechts der Isar, Technical University of Munich, Munich, Germany

[‡] Medizinische Klinik und Poliklinik, Universitätsklinikum Hamburg-Eppendorf, Hamburg, Germany

[§] Department of Pathology and Immunology, Division of Clinical Pathology, University of Geneva, Genève, Switzerland

[¶] Center of Allergy and Environment (ZAUM), Helmholtz Center and Technical University of Munich, Munich, Germany

[‖] Institute for Immunology, Biomedical Center, Ludwig-Maximilians-University Munich, Munich, Germany

[#] Munich Cluster for Systems Neurology (SyNergy), Munich, Germany

Running title: α4 integrins in DC accumulation in CNS and gut

Character count including spaces (not including estimates for figures): 63,150

[2] Correspondence: Thomas Korn, Klinikum rechts der Isar, Technical University of Munich, Ismaninger Str. 22, 81675 Munich, Germany; Phone: ++49-89-41405617; Fax: ++49-89-41404675; E-mail: thomas.korn@tum.de

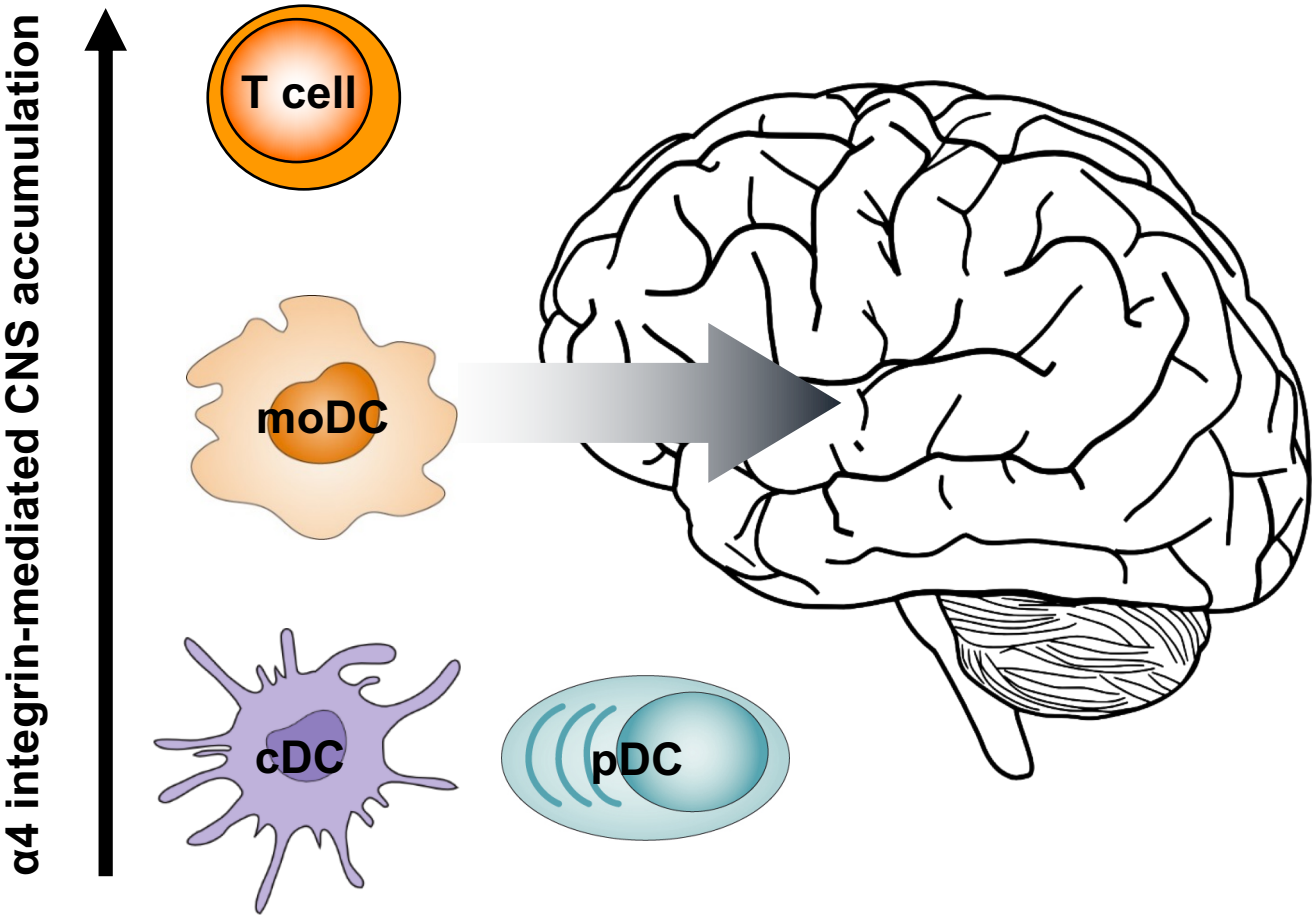
α4 integrin-mediated CNS accumulation
T cell
moDC
cDC
pDC

Abstract

Homing of pathogenic $CD4^+$ T cells to the central nervous system (CNS) is dependent on α4 integrins. However, it is uncertain whether α4 integrins are also required for the migration of dendritic cell (DC) subsets, which sample antigens from non-lymphoid tissues to present it to T cells. Here, after genetic ablation of *Itga4* in DCs and monocytes in mice via the promoters of *Cd11c* and *Lyz2* (also known as LysM), respectively, the recruitment of α4 integrin-deficient conventional and plasmacytoid DCs to the CNS was unaffected while α4 integrin-deficient monocyte-derived DCs (moDCs) accumulated less efficiently in the CNS during experimental autoimmune encephalomyelitis in a competitive setting than their wild-type counterparts. In a non-competitive setting, α4 integrin deficiency on moDCs was fully compensated. In contrast, in small intestine and colon, the fraction of α4 integrin-deficient $CD11b^+CD103^+$ DCs was selectively reduced in steady state. Yet, T cell mediated inflammation and host defense against *Citrobacter rodentium* were not impaired in the absence of α4 integrins on DCs. Thus, inflammatory conditions can promote an environment that is indifferent to α4 integrin expression by DCs.

Key words: α4 integrin / dendritic cells / intestinal lamina propria / EAE / *Citrobacter rodentium*.

Key points

1. α4 integrins are dispensable for cDCs and pDCs to populate the CNS in steady state.

2. *Itga4*$^{-/-}$ moDCs have a competitive disadvantage to accumulate in the inflamed CNS.

3. Accumulation of CD11b^{+}CD103^{+} DCs in gut lamina propria is dependent on α4 integrins.

Introduction

$CD11c^+$ myeloid cells are present in the non-inflamed CNS. Both juxtavascular and intraparenchymal localization of $CD11c^+$ cells have been demonstrated in the CNS in steady state (1, 2). Although perivascular MHC class II expressing cells were initially termed "perivascular microglia" (3), it is now clear that they are distinct from proper intraparenchymal microglial cells (4-6). While intraparenchymal $CD11c^+$ cells are likely microglial cells that are dispensable for the presentation of antigens to T cells, perivascular $CD11c^+$ cells are of hematopoietic origin and serve a non-redundant role for the stimulation of T cells in the CNS in steady state and during inflammation (7-10).

A series of recent studies have addressed the provenance and maintenance of perivascular and meningeal $CD11c^+$ cells within the CNS compartment (10-12). Similarly as in T cells, integrin expression in DCs has been proposed to mediate firm adhesion of DCs to CNS endothelial cells as a prerequisite for their transmigration into the CNS compartment. While in some studies, $\alpha 4\beta 1$ integrin (VLA-4) was found to mediate DC adhesion to endothelial cells (13), other reports stressed the importance of $\alpha L\beta 2$ integrin (LFA-1) in transmigration of DCs across the inflamed endothelial barrier (14). In addition, it appears that pre-cDCs migrate to the meningeal and perivascular compartment in steady state, become mature DCs and stay *in situ* with a half life of 5-7 days (15).

Limited information exists as to the fraction of plasmacytoid DCs (pDCs) and conventional DCs (cDCs) within the CNS DC compartment. In particular, pDCs were regarded as gate keepers of immunologic homeostasis due to their potential tolerogenic functions (16).

Immature pDCs were even considered for adoptive immune therapeutic approaches to re-install immune homeostasis in autoimmune neuroinflammation (17). Yet, given their role as primary sources of type I interferons in response to foreign DNA stimulation, the role of pDCs in priming and maintaining encephalitogenic T cell responses is controversial and both proinflammatory functions of pDCs as well as tolerizing functions of pDCs were reported. While anti-PDCA-1 mediated depletion of pDCs prior to immunization decreased EAE, delayed ablation of pDCs exacerbated the disease course (18). The mechanism how pDCs induce tolerance is elusive and various mechanisms including selective expansion of $Foxp3^+$ Treg cells in an antigen specific manner have been discussed (16). The functional diversity of cDCs is only beginning to be understood (19): A recent concept proposed that distinct subsets of cDCs induce distinct phenotypes of T cell responses (20). For example, in the gut lamina propria, $CD11b^+CD103^-$ and $CD11b^+CD103^+$ DCs (cDC2s) promote Th17 responses (21) while $CD11b^{low}CD103^+$ DCs induce Th1 responses and are particularly proficient in cross presenting exogenous antigens to $CD8^+$ T cells (22-24).

Since the cerebrospinal fluid (CSF) and CNS parenchyma were depleted of DCs in Multiple sclerosis (MS) patients receiving a blocking antibody to α4 integrins, VLA-4 has been believed to control the access of DCs to the CNS compartment under inflammatory conditions in humans as well. The depletion of the CNS antigen presenting cell (APC) compartment due to administration of an anti-VLA-4 antibody (natalizumab) has also been blamed for the loss of immune surveillance and failure to control JC virus infection resulting in progressive multifocal leukencephalopathy (25). After termination of natalizumab treatment, antibody-desaturation of VLA-4 on immune cells takes about 10 weeks (26). Yet, the depletion of T cells in the CSF compartment is prolonged until 6 – 12 months after stopping natalizumab, suggesting that

indirect effects such as the reduction of APCs in the CSF space and the CNS parenchyma during and after natalizumab treatment might contribute to the delayed repletion of the CSF space with T cells (27).

Using a genetic model, this study was designed to investigate the role of α4 integrins (encoded by *Itga4*) in DC subsets for populating the intracerebral APC niche during development, in homeostasis, and under inflammatory conditions. Complete ablation of *Itga4* both in pDCs and cDCs did not affect the overall antigen presenting capacity of the CNS compartment in steady state nor the accumulation of DCs in the CNS during inflammation. In the small intestinal lamina propria, the fraction of $CD11b^+$ cDC2s was significantly decreased in DC conditional α4 integrin-deficient mice in homeostasis. However, priming of protective Th17 responses was still sufficient in *Citrobacter rodentium* infection. We propose that α4 integrins on DCs do not directly control the trafficking of DCs into the CNS and are redundant for the recruitment of DCs into the gut lamina propria during inflammation.

Materials and Methods

Mice

2D2 MOG(35-55) TCR specific transgenic mice (28) crossed with Foxp3-GFP knock-in mice (29) and *Itga4*$^{flox/flox}$ mice (30) have been previously described. CD11c Cre (31), CD11c-GFP Cre (32), and LysM Cre deleter strains (33) were obtained from Jackson laboratories. All mouse strains were on pure C57BL/6 genetic background. Mice were kept in specific pathogen free conditions at the Technical University of Munich or the University Hospital Hamburg Eppendorf in accordance with the local regulations for animal experimentation (Az ROB-55.2-2532.Vet_02-13-29 and ROB-55.2-2532.Vet_03-18-53, Bavarian State Authorities, Munich, Germany and Az 28/14 'Behörde für Soziales, Familie, Gesundheit und Verbraucherschutz' Hamburg, Germany).

Induction of EAE

To induce EAE, mice were immunized *s.c.* (base of tail) with 200 µl of an emulsion containing 200 µg MOG(35-55) (MEVGWYRSPFSRVVHLYRNGK; Auspep, Tullamarine, Australia) and 500 µg *M. tuberculosis* H37Ra (BD Difco) in CFA and received 200 ng PTX (Sigma) i.v. on the same day and 2 days after the immunization. Clinical signs of disease were monitored as described previously (34).

Adoptive transfer EAE

For adoptive transfer experiments, C57BL/6 wild-type donor mice were immunized with MOG(35-55) peptide in CFA and PTX according to the regimen for active induction of EAE. On day 7, draining lymph nodes and spleens were prepared, pooled and *ex vivo* re-stimulated for 3 days with 35 μg/ml MOG(35-55) in the presence of TGF-β (0.25 ng/ml), IL-6 (5 ng/ml), IL-23 (6.5 ng/ml) as well as anti-IFN-γ (10 μg/ml) in order to skew antigen specific T cells into Th17 cells. After isolation of $CD4^+$ T cells from the recall culture using Miltenyi untouched $CD4^+$ T cell purification beads, 6 x 10^6 $CD4^+$ T cells were transferred i.v. into recipient mice, concomitantly with intraperitoneal injection of PTX on days 0 and 2 after adoptive transfer.

Expansion of DCs *in vivo*

B16 Flt3L-secreting melanoma cells were cultured and implanted as previously described (35). Briefly, cells were cultured in supplemented RPMI 1640 at 37°C and 5% CO_2 for at least 3 days, subconfluently harvested and subcutaneously injected in the neck at 6 x 10^6 cells in PBS per mouse. Mice were sacrificed after 7 days and dendritic cells were isolated as described below.

Generation of mixed bone-marrow chimeras

Mice were irradiated at a dose of 11 Gray. A total of 10-20 x 10^6 donor bone marrow cells mixed 1:1 from CD45.1 wild type donors and indicated knock-out mice, depleted of $CD90.2^+$ cells using Miltenyi Microbeads, were injected i.v. into recipients within 16-20 h post irradiation. The reconstituted mice were maintained on antibiotic water (Enrofloxacin, Bayer, 0.1 mg/ml) for 3

weeks after transplantation. The reconstitution of the hematopoietic compartment was checked 5-6 weeks post cell transfer in peripheral blood.

In vivo LFA-1 blockade

For in vivo blockade experiments, MOG(35-55)–immunized mice were treated with i.p. injections of anti-LFA-1 antibody (M17/4, Bioxcell) or Rat IgG2a isotype control (clone 2A3, Bioxcell) in PBS starting on day 5 (200 µg), followed by i.p. injections of 100 µg every other day until day 15 after immunization. Shortly after, mice were analyzed at peak disease.

Injection of anti-CD3 antibody

Mice were injected intraperitoneally with 20 µg of anti-CD3e (clone 2C11, Bioxcell) in PBS on d0, d2, and d4 and weighed daily for a total of 7 days.

C. rodentium infection

Luciferase-expressing, nalidixic acid-resistant derivative of *C. rodentium* (ICC180) was grown overnight in Lysogeny broth (LB) containing 50 µg/ml of nalidixic acid with shaking at 37ºC. Next day, the suspension of bacteria was washed twice with PBS and the concentration was adjusted to 5 x 10^9 cfu/ml. Mice were infected by oral gavage with 0.2 ml of *Citrobacter rodentium* solution containing 1 x 10^9 cfu. On day 7 post-infection, mouse colon and caecum were dissected as described below, fecal material was dissolved in PBS and seeded in serial dilutions on LB agar plates with nalidixic acid for 24 h at 37 °C followed by counting of

colonies. These experiments were approved by the institutional review board 'Behörde für Soziales, Familie, Gesundheit und Verbraucherschutz' (Hamburg, Germany).

Histology

Mice were perfused with cold PBS followed by 4% paraformaldehyde fixation (pH 7.4). Brain and spinal cord were dissected and embedded in paraffin. Antigen retrieval was performed on 3 µm thick sections according to standardized protocols by heating with citrate buffer (pH6). Endogenous peroxidases (peroxidase blocking reagent, Dako) were neutralized and unspecific binding blocked for 5 min (PBS/1% BSA/2% FCS). For immunofluorescence, sections were blocked for 5 min (PBS/1% BSA/2% FCS) and subsequently incubated with monoclonal rat anti-GFP (clone FM264G, Biolegend). Bound antibodies were visualized with AlexaFluor-488-labeled goat anti-rat IgG (ThermoFisher). Subsequently, sections were incubated with polyclonal rabbit anti-mouse CD3 (Dako) and visualized with AlexaFluor-647-labeled donkey anti-rabbit secondary antibody. Immunostained sections were scanned using Pannoramic Digital Slide Scanner 250 FLASH II (3DHistech) in 200x magnification.

Preparation of mononuclear cells

At the peak of disease, CNS-infiltrating cells were isolated after perfusion through the left cardiac ventricle with PBS. Brain and spinal cord were extracted and meningeal layers of the spinal cord stripped under microscopic dissection. Tissues were digested with collagenase D (2.5 mg/ml) and DNase I (1 mg/ml) at 37°C for 45 min. After passing the tissue through a 70 µm cell

strainer, cells of the spinal cord and brain were separated by discontinuous Percoll gradient (70%/37%) centrifugation. Mononuclear cells were isolated from the interphase.

Isolation of lamina propria mononuclear cells

Peritoneal cavity was opened, mesenteric lymph nodes were retrieved and small and large intestines were dissected and cleaned with HBSS on ice. Fat and Peyer's patches (if applicable) were removed and intestinal contents flushed with HBSS. Intestines were cut into segments of 5 mm, washed in HBSS and epithelial layers removed by shaking in HEPES-buffered HBSS containing 0.25 mM EDTA at 37 °C for 30 min, followed by repetitive washing in HBSS. Cells were extracted by incubation with DNase I (0.2 mg/ml) and Liberase TL (0.17 mg/ml) at 37°C for 15 min, followed by inactivation using RPMI 1640 supplemented with 10% FCS. Suspension and remaining tissue were forced through a 100 µm cell strainer, washed in RPMI 1640 and subjected to 37% Percoll purification, with mononuclear cells being retrieved from the pellet. Mesenteric lymph nodes were digested with collagenase D (2.5 mg/ml) and DNase I (1 mg/ml) at 37 °C for 30 min and passed through a 70 µm cell strainer.

***In vivo* proliferation of antigen specific T cells**

Lymph nodes and spleens from naïve 2D2 x Foxp3–GFP mice were isolated, pre-enriched using Miltenyi CD4 (L3T4) purification beads and sorted for $CD44^{-}Foxp3\ (GFP)^{-}$ cells on a MoFlo II cell sorter. Obtained cells were labeled using eBioscience Cell Proliferation Dye eFluor 450 and $3x10^6$ labeled CD4 T lymphocytes were injected i.v. into recipient mice. 24h later, mice were immunized with MOG(35-55) peptide as described above. Cells were reisolated from draining

axillary and inguinal lymph nodes 4 days after immunization and dilution of proliferation dye was assessed by flow cytometry. Proliferation index was calculated with R version 3.5.3 (R Core Team, 2019) using the package flowFit version 1.20.1 (36).

Intracellular cytokine staining and flow cytometry

Cells were stained with live/dead fixable dyes (Aqua [405 nm exc], Invitrogen) and antibodies to surface markers: CD3e (145-2C11), CD4 (GK1.5 or RM4-5), CD8a (53-6.7), CD11b (M1/70), CD11c (HL3), CD19 (1D3 or 6D5), CD44 (IM7), CD45 (30-F11), CD45.1 (A20), CD45.2 (104), CD45R (B220; RA3-6B2), CD49d (a4 integrin, 9C10/MFR.4.B), CD64 (X54-5/7.1), Thy1.1 (CD90.1, Ox-7), CD103 (2E7), CD115 (AFS98), CD135 (FLT3; A2F10), CD317 (BST-2; eBio927), CD172 (SIRPα, P84), 2D2 TCR Vα3.2 (RR3-16) and Vβ11 (RR3-15), F4/80 (BM8), Ly6G (1A8), Ly6C (HK1.4), MHC II (M5/114.15.2), NK1.1 (PK136), Siglec H (eBio440c), XCR-1 (ZET); all BD Biosciences, eBioscience or BioLegend. For intracellular cytokine staining, cells were re-stimulated with 50 ng/ml PMA (Sigma-Aldrich), 1 µg/ml ionomycin (Sigma-Aldrich) and monensin (1 µl/ml BD GolgiStop) at 37 °C for 2.5 h. Subsequent to live/dead and surface staining, cells were fixed and permeabilized (Cytofix/Cytoperm and Perm/Wash Buffer; BD Biosciences), and stained for cytokines IL-17A (TC11-18H10.1; BioLegend), IFN-γ (XMG1.2, eBioscience), and GM-CSF (MP1-22E9, BD Biosciences). Intranuclear stainings for Foxp3 (FJK-16s), IRF8 (V3GYWCH), RORγt (AFKJS-9), Gata3 (TWAJ) and Helios (22F6) were performed using the Transcription Factor Staining Set (eBioscience). Cells were analyzed using a CyAn ADP 9 flow cytometer (Beckmann/Coulter) and a CytoFlex S (Beckmann Coulter). Cell counting was performed by a Guava easyCyte 5HT cytometer (Merck) together with 7-AAD (BD), Fixable Red Dead Cell Stain (ThermoFisher), or

Fixable Viability Dye eFluor 520 (eBioscience) and CD45 (30-F11) or CD45.2 (104). All data analysis was facilitated using FlowJo version 10 (Tree Star). For intravascular staining, mice were injected i.v. with 1 µg of CD45.2 (104) or CD45 (30-F11) in 200 µl PBS, 5 min before sacrificing.

Quantification and statistical analysis

Statistical evaluations of cell frequency measurements and cell numbers were performed by one-way ANOVA followed by Tukey's multiple comparisons test when three genotypes of a single cell population were compared, by one-way ANOVA followed by Sidak's multiple comparison test when two genotypes of multiple cell populations were compared, or by two-way ANOVA followed by Sidak's multiple comparisons test when three genotypes of multiple cell populations were compared, as indicated in the figure legends. MBMC ratios were compared to the indicated reference population for any given organ using one-way ANOVA followed by Dunnett's multiple comparisons test. Multiplicity adjusted p values < 0.05 were considered significant. Differences of same-day littermate analyses for the gut were evaluated using two-tailed, paired Student's tests. EAE scores between groups were analyzed as disease burden per individual day with one-way ANOVA and Dunnett's post-hoc test. Body-weight loss was assessed by two-way ANOVA followed by Sidak's multiple comparisons test. *Citrobacter* CFU was compared using a two-tailed, unpaired Student's t test. Survival curves were analyzed by Log-rank (Mantel-Cox) test. Statistical analysis was performed in Graphpad Prism 8.1.0 (Graphpad Software, Inc).

Results

Genetic ablation of *Itga4* in DCs has no effect on the DC niche in the CNS

In order to test whether genetic ablation of *Itga4* in $CD11c^+$ cells interfered with the establishment of a functional antigen presenting cell-niche within the CNS, we crossed CD11c Cre (31) or CD11c-GFP Cre mice (32) with $Itga4^{flox/flox}$ mice (30) to generate DC conditional α4 integrin-deficient mice, termed $Itga4^{\Delta DC}$. The ablation of *Itga4* was highly efficient in $CD11c^+$ cells in the spleen in steady state (Suppl. Fig. 1A), and even pre-cDC precursors in the bone marrow were efficiently ablated of α4 integrin expression (Suppl. Fig. 1B). The CD11c Cre deleter strain (31) is known to also affect non-DC immune cell populations to varying degrees across different floxed alleles (37, 38). Therefore, we tested for α4 integrin mosaics in lymphoid and myeloid populations of $Itga4^{\Delta DC}$ mice and confirmed this prior observation (Suppl. Fig. 1C). However, while *Itga4* ablation was complete in DCs, recombination was only partial in non-DC immune cell populations (Suppl. Fig. 1C).

In the CNS, the distribution of $CD11c^+$ cells in the meninges, plexus choroideus and perivascular space was identical in $Itga4^{\Delta DC}$ and CD11c Cre x $Itga4^{flox/wt}$ control mice (Fig. 1A). Using a gating strategy with established markers (Fig. 1B), we identified within the $CD11c^+$MHC class II^+ gate, pDCs (BST-2^+), cDC1s ($CD11b^-CD103^+$), and cDC2s ($CD11b^+CD103^-$) in the CNS in steady state (Fig. 1B) and in "elevated homeostasis" after Flt3L treatment, which expands $CD11c^+$ cells *in vivo* under non-inflammatory conditions (15) (Suppl. Fig. 1D). These data suggested that the expression of α4 integrins on $CD11c^+$ cells was

dispensable for the recruitment and maintenance of DCs or CD11c^{+}MHC class II^{-} DC precursor cells into the CNS niche in steady state.

In order to test whether α4 integrin expression on DCs was required for their presence in the CNS in a competitive setting, mixed bone marrow chimeras were generated by grafting a 1:1 mixture of wild-type (CD45.1) and *Itga4*$^{\Delta DC}$ bone marrow into irradiated matched knock-out recipients. After full reconstitution of the peripheral immune compartment, the CNS was analyzed. Here, we observed an equal distribution of pDCs, cDC1s, and cDC2s in the wild-type and the *Itga4*$^{\Delta DC}$ compartment in the CNS of mixed bone marrow chimeras both in steady state (Fig. 1C) and after Flt3L treatment (Fig. 1D). Together, these data indicated that no gross alteration of the CNS DC compartment resulted from genetic ablation of *Itga4* in CD11c^{+} cells.

Disease severity in active EAE is not affected by ablation of *Itga4* in myeloid cells

Next, we wanted to test whether constitutive ablation of *Itga4* in DCs had an effect on autoimmune neuroinflammation. In addition to *Itga4*$^{\Delta DC}$ mice, we ablated *Itga4* in both DCs and monocytes using a combined CD11c Cre and LysM Cre deleter strain. Along with *Itga4*$^{flox/flox}$ control mice, *Itga4*$^{\Delta DC}$ mice as well as mice with constitutive ablation of *Itga4* in both DCs and monocytes (*Itga4*$^{\Delta DC\Delta Mo}$) were immunized with MOG(35-55) in CFA for induction of EAE. Both conditional knock-out strains developed clinical disease with similar kinetics and severity as *Itga4*$^{flox/flox}$ control mice (Fig. 2A). We tested the quantity and the quality of the antigen specific T cell response in *Itga4*$^{\Delta DC}$ mice by transferring MOG TCR transgenic reporter cells (2D2) into either control mice (*Itga4*$^{flox/flox}$) or *Itga4*$^{\Delta DC}$ mice followed by immunization with MOG(35-55) in CFA. After 4 days, the proliferation of 2D2 cells re-isolated from the draining lymph nodes

was similar in control and *Itga4*$^{\Delta DC}$ mice (Suppl. Fig. 2A), indicating that the priming of antigen specific T cells in the peripheral immune compartment was unaltered in *Itga4*$^{\Delta DC}$ mice upon active immunization with MOG(35-55) in CFA. The identical course of disease in control mice and *Itga4*$^{\Delta DC}$ mice already suggested that the restimulation of encephalitogenic T cells within the CNS compartment was not impaired. Indeed, we did not observe relevant differences either in the fraction of Foxp3^{+} Treg cells (Suppl. Fig. 2B) or in the profile of effector cytokines in CD4^{+} T cells isolated from the CNS of control mice, *Itga4*$^{\Delta DC}$ mice or *Itga4*$^{\Delta DC\Delta Mo}$ mice at the peak of EAE (Suppl. Fig. 2C).

To exclude an alteration of the APC composition that is only functionally redundant with regard to downstream T cell effects, we analyzed the DC compartment in the inflamed CNS of control mice as compared with *Itga4*$^{\Delta DC}$ mice or *Itga4*$^{\Delta DC\Delta Mo}$ mice in detail. During inflammation, our gating strategy allowed for the differentiation of pDCs and cDC1s (Fig. 2B). In contrast to steady state where essentially no moDCs were detected in the CNS (Suppl. Fig. 2D), cDC2s could no longer be unequivocally distinguished from moDCs in EAE, both expressing high levels of CD64 under inflammatory conditions. CNS-derived cDC1s did not express CD64 and were Irf8^{+} while moDCs lacked Irf8 (Suppl. Fig. 2E). *Itga4* was efficiently ablated in pDCs and cDC1s in *Itga4*$^{\Delta DC}$ mice while moDCs were partly spared from *Itga4* ablation (Fig. 2B). Notably, *Itga4* ablation was highly efficient in all DC subsets including pDCs, cDC1s, and moDCs in *Itga4*$^{\Delta DC\Delta Mo}$ mice (Fig. 2B). In contrast to DC subsets, CD11b^{+}CD45^{int} microglial cells did not express α4 integrins (Fig. 2B). The fractions and absolute numbers of pDCs, cDC1s, and moDCs in the inflamed spinal cord, brain, and meninges of EAE mice were similar in *Itga4*$^{\Delta DC}$ mice and *Itga4*$^{\Delta DC\Delta Mo}$ mice as compared to control animals (Fig. 2C, Suppl. Fig. 2F), suggesting that lack of α4 integrin expression can be compensated as to the recruitment

of DC subsets into the inflamed CNS. Of note, the lack of differences in moDC infiltration was not due to a lack of deletional efficiency in progenitors (as reported for the LysM Cre deleter strain in the context of other floxed alleles (39)) since inflammatory monocyte progenitors in the blood post-immunization already exhibited efficient and functional deletion of the floxed α4 allele in *Itga4*$^{\Delta DC\Delta Mo}$ mice prior to infiltrating the CNS (Suppl. Fig. 2G).

LFA-1, an αLβ2 integrin heterodimer, had previously been reported to be dispensable for the recruitment of endogenous myeloid cells in adoptive transfer EAE (40-42). Here, we asked whether in the absence of α4 integrin expression on DCs, LFA-1 might become non-redundant for the accumulation of DCs in the CNS during EAE. However, when we blocked LFA-1 with a monoclonal antibody to CD11a in *Itga4*$^{\Delta DC}$ mice as of day 5 after immunization with MOG(35-55), we failed to protect the mice from clinical disease, and the fractions and numbers of DC subsets in the CNS of anti-CD11a treated *Itga4*$^{\Delta DC}$ mice were similar to control treated *Itga4*$^{\Delta DC}$ mice (Suppl. Fig. 2H), suggesting that LFA-1 was irrelevant for the CNS-recruitment of α4 integrin-deficient DCs.

Next, we wanted to test the significance of α4 integrins in CD11c^{+} cells in a competitive setting during inflammation. Again, we constructed bone marrow chimeras and grafted congenically marked wild-type bone marrow (CD45.1^{+}) together with either *Itga4*$^{\Delta DC}$ bone marrow (CD45.2) or *Itga4*$^{\Delta DC\Delta Mo}$ bone marrow (CD45.2) into recipient mice and subjected them to EAE. Consistent with the clinical data, CD11c^{+} cells deficient in α4 integrins did not show an impaired seeding of the CNS niche during inflammation even in direct competition with their wild-type counterparts (Fig. 2D). In contrast, lack of α4 integrin-expression on moDCs (in the *Itga4*$^{\Delta DC\Delta Mo}$ APC compartment) rendered CD11c^{+}CD11b^{+} moDCs less fit than their α4 integrin-

sufficient counterparts in populating the CNS during inflammation (Fig. 2E). Together, these data suggested that – despite the partial requirement of α4 integrins for the recruitment of moDCs into the CNS – α4 integrin expression on *bona fide* pDCs and cDCs was dispensable for establishing a functional antigen presenting compartment in the CNS for full activation of autoreactive T cells *in situ*.

In situ restimulation of encephalitogenic T cells is fully functional in *Itga4*$^{\Delta DC}$ mice

In order to more specifically probe the APC capacity of the CNS in our various α4 integrin deficient strains, we performed adoptive transfer of exogenously primed Th17 cells into either *Itga4*$^{flox/flox}$ control mice, *Itga4*$^{\Delta DC}$ or *Itga4*$^{\Delta DC\Delta Mo}$ mice. Again, incidence, kinetics, and severity of adoptive transfer EAE in the knock-out strains were similar to those in control recipients (Fig. 3A). Neither, did we notice any significant difference in the fractions or absolute numbers of spinal cord- or brain-derived pDCs, cDCs, or moDCs (Fig. 3B, Suppl. Fig. 3A), or in the fraction of Foxp3$^+$ Treg cells or in the profile of effector cytokines of CD4$^+$ T cells re-isolated from the CNS (Suppl. Fig. 3B, C) of *Itga4*$^{\Delta DC}$ or *Itga4*$^{\Delta DC\Delta Mo}$ mice as compared to control recipients at the peak of adoptive transfer EAE. In summary, our data indicated that lack of α4 integrins in the DC compartment did not abrogate or even impair the competence of the intrathecal APC compartment to induce and maintain antigen specific T cell responses.

CD11b$^+$CD103$^+$ DCs are reduced in the lamina propria of *Itga4*$^{\Delta DC}$ mice

α4 integrins are key homing molecules for immune cells into the gut lamina propria (43). Therefore, we asked whether the gut DC compartment was changed in *Itga4*$^{\Delta DC}$ mice, in which

all *bona fide* DC populations exhibited efficient deletion of α4 integrin (Suppl. Fig. 4A). In steady state, we found decreased fractions of $CD103^+CD11b^+$ double positive DCs and increased fractions of $CD103^+CD11b^-$ single positive DCs in the small intestinal as well as in the colonic lamina propria of $Itga4^{\Delta DC}$ mice as compared to $Itga4^{flox/flox}$ control mice (Fig. 4A), suggesting that double positive DCs were most dependent on α4 integrins for populating the intestinal lamina propria. In a competitive setting of mixed bone marrow chimeras that had received a 1:1 mixture of wild-type (CD45.1) and $Itga4^{\Delta DC}$ (CD45.2) bone marrow, the distribution of all wild-type and $Itga4^{\Delta DC}$ DC subsets was even in the spleen (Fig. 1C), but shifted in favor of wild-type DCs in particular in the $CD103^+CD11b^+$ double positive cDC compartment in the small intestinal and colonic lamina propria, but not in the mesenteric lymph nodes (Fig. 4B). Thus, α4 integrins were required for the accumulation of double positive DCs in the gut lamina propria.

α4 integrins in DCs are dispensable for host defense against *C. rodentium*

In the gut, double positive DCs were proposed to be required for both, the induction of pTregs that contribute in maintaining immune tolerance against commensal gut bacteria, as well as the priming of protective Th17 responses against pathogens and pathobionts. First, we tested the frequencies of pTregs in the gut that are characterized by the co-expression of Foxp3 and RORγt (44) in steady state. We noticed a slight tendency towards lower fractions of $ROR\gamma t^+Helios^-$ Treg cells in the small intestinal lamina propria of $Itga4^{\Delta DC}$ mice as compared to $Itga4^{flox/flox}$ control animals (Suppl. Fig. 4B).

Next, we assessed acute inflammatory responses in the gut in response to intraperitoneal injection of an activating antibody to CD3 (45), which has been shown to induce Th17 responses

in the small intestine. The clinical phenotype (weight loss, Fig. 5A) was similar in wild-type littermate controls and *Itga4*$^{\Delta DC}$ mice. These data indicated that the priming of Th17 cells (which have been shown to drive the pathology in this model (45)), can occur with residual amounts of double positive DCs. Finally, we investigated *C. rodentium* infection, an infectious disease model, which is in part dependent on antigen specific Th17 cells (46). Upon *C. rodentium* infection, wild-type and *Itga4*$^{\Delta DC}$ mice cleared the pathogen equally well (Fig. 5B, C). Consistent with the clinical observation, the clear reduction of double positive cDCs in the lamina propria of the colon that was eminent in steady state was entirely recovered in inflammation (Fig. 5D), again suggesting that redundant mechanisms can compensate for the lack of α4 integrins on DCs as to their recruitment to sites of inflammation. In summary, the altered DC compartment in *Itga4*$^{\Delta DC}$ mice in the gut did not translate into gross changes of resilience to inflammatory or infectious perturbations at least in the tested disease models.

Discussion

In this study, we tested the requirement of α4 integrin expression on $CD11c^+$ cells for the seeding of CNS and intestinal niches with $CD11c^+$MHC class II^{high} DCs in steady state and for the recruitment of DCs during autoimmune inflammation of the CNS and host defense in the gut. While the expression of α4 integrins was largely irrelevant for the replenishment of CNS DCs, the gut-specific population of $CD11b^+CD103^+$ DCs was diminished in *Itga4*$^{\Delta DC}$ mice. However, in an infection model with attaching and effacing bacteria, the reduction of this DC population in the colonic lamina propria did not result in an adverse outcome as compared to wild-type control animals. Thus, α4 integrin expression on DCs is a redundant feature in the settings addressed in this study. Differences in the composition of DC populations in *Itga4*$^{\Delta DC}$ mice vs control mice in homeostasis were functionally compensated under inflammatory conditions.

CNS DCs are of hematopoietic origin, and compelling evidence indicates that the capacity to present antigen to T cells *in vivo* is restricted to these $CD11c^+$ cells, while microglial cells are unable to present antigens to T cells (3, 9, 10). Moreover, depletion experiments of DCs using the diphtheria toxin receptor system expressed either in $CD11c^+$ or $Zbtb46^+$ cells have provided strong evidence that the physical presence of DCs in the CNS is required for the productive restimulation of incoming autoreactive T cells (47). The CNS niche is seeded with pre-cDCs that then differentiate into distinct DC subsets *in situ* (15). In line with previous studies (1, 48, 49), we here showed that the steady state CNS DC compartment consisted of pDCs ($BST2^+SiglecH^+$), $CD11b^{low}CD103^+$ cDC1s, and $CD11b^+CD103^-$ cDC2s but not moDCs. Flt3L application expanded all DC subsets in the CNS but did not change their relative composition, indicating that moDCs (or TipDCs (50) or $CD11c^+$MHC class II^+ monocytes), which do not

respond to Flt3L-driven expansion (15, 48), did not contribute to the DC compartment in the CNS during homeostasis. Notably, the process of Flt3L-mediated DC expansion in the CNS was independent of α4 integrin expression by DCs. Also, *Itga4* was as efficiently ablated in pre-cDCs as in pDCs, cDC1s, and cDC2s in *Itga4*$^{\Delta DC}$ mice. Thus, it is unlikely that pre-cDCs seed the CNS niche in a VLA-4 dependent manner and only then lose α4 integrin expression *in situ*. In fact, none of the steady state DC subsets (including pre-cDCs) depended on α4 integrins in order to populate the CNS niche including meninges and choroid plexus, and *Itga4*$^{\Delta DC}$ mice disposed of a fully replete CNS DC niche. Consistent with these results, restimulation of incoming T cells in the CNS compartment was not altered in *Itga4*$^{\Delta DC}$ mice. These results are in line with prior reports that only physical depletion of CD11c^{+} DCs cells or Zbtb46^{+} cDCs from the steady state CNS is associated with impaired local restimulation of autoreactive T cells (47).

In inflammation, VLA-4 expression on pDCs or cDC1s was dispensable for their CNS recruitment since ablation of *Itga4* did not put CD11c^{+} cells at a disadvantage to migrate to the inflamed CNS as compared to their wild-type counterparts. CD11c Cre mice showed a complete recombination and thus total loss of α4 integrin expression in all DC subsets. As has been reported before, CD11c Cre resulted in partial ablation of the floxed allele in lymphoid cells as well. However, the α4 integrin mosaic in T cells of *Itga4*$^{\Delta DC}$ mice was functionally irrelevant because wild-type T cells and T cells from *Itga4*$^{\Delta DC}$ mice behaved in an identical manner during EAE. We did not observe any signs of atypical EAE in *Itga4*$^{\Delta DC}$ mice - a phenotype which has been reported in T cell conditional α4 integrin deficient mice (51).

Interestingly, moDCs depended (at least in part) on the expression of α4 integrins for their recruitment into the inflamed CNS when wild-type and α4 integrin deficient moDCs

competed with each other for the CNS niche in chimeras reconstituted with wild-type plus *Itga4*$^{\Delta DC\Delta Mo}$ mixed bone marrow. MoDCs are the major effector cells during EAE, are expanded and shaped by GM-CSF and guided to the CNS in a CCR2 dependent manner (39, 52, 53). However, the α4 integrin-dependent recruitment of moDCs to the CNS was redundant and was overcome during inflammation in *Itga4*$^{\Delta DC\Delta Mo}$ mice in a non-competitive setting. In line with these results, a previous report suggested that expression of β1 integrin, the partner of α4 integrin to form heterodimeric VLA-4, was dispensable for the recruitment of myeloid cells into the inflamed CNS (54). Yet, later work suggested that immature dendritic cells need α4 integrins in order to home to the CNS meningeal space and white matter parenchyma (13). While these conclusions are based on bone marrow-derived DCs that were either deficient in β1 integrin or exposed to anti-VLA4 antibodies *in vitro* prior to adoptive transfer into host mice with EAE, we here show by genetic ablation of *Itga4* in DCs, that endogenous DCs can still migrate into the CNS in the absence of α4 integrin expression. Interestingly, LFA-1 has been reported to be dispensable for the recruitment of myeloid cells into the CNS in adoptive transfer EAE (40-42) while in Toxoplasma infection, antibody-blockade of LFA-1 reduced the accumulation of adoptively transferred DCs in the CNS (14). Here, we provided evidence that LFA-1 failed to become a non-redundant mediator of DC recruitment during EAE of *Itga4*$^{\Delta DC}$ mice. Thus, DCs accumulated in the inflamed CNS despite simultaneous dysfunction of the VLA4/VCAM1 and LFA-1/ICAM1 pathways, suggesting that the requirements for DC recruitment to the CNS in autoimmunity may differ from T cell recruitment (51) and rely on alternative integrin interactions.

Our data enable a more informed interpretation of the finding that the amount of DCs in the perivascular space of natalizumab treated MS patients was reduced (25). A long term failure

of immune surveillance of the CNS had been proposed since the lack of APCs in the perivascular space would no longer licence incoming T cells to patrol the CNS parenchyma. Our observation that DCs are not crucially dependent on α4 integrins for their accumulation in the perivascular and meningeal compartments now suggests that the prolonged depletion of the CNS perivascular space of DCs in natalizumab treated patients is not a direct effect of α4 integrin blockade on DCs. Either the turn-over of DCs in the perivascular space is very low, as has been previously suggested in mouse models (11) or - by prior treatment with natalizumab - intrinsic properties of the perivascular niche are changed that would prevent the migration and replenishment of DCs.

Contrary to the CNS compartment, the expression of α4 integrins by $CD11b^+CD103^+$ DCs is required for their maintenance in the lamina propria of the intestine, yet less in the mesenteric lymph nodes. In the gut, $CD11b^+CD103^+$ DCs are Irf4 dependent (21) and are required for the induction of microbiota specific pTreg cells in the lamina propria and mesenteric lymph nodes (55-57) and the priming of Th17 responses in mesenteric lymph nodes (58). Since in steady state, ablation of *Itga4* on $CD11c^+$ cells led to a reduced number (but not complete absence) of $CD11b^+CD103^+$ DCs in the lamina propria, the fraction of $ROR\gamma t^+$ Treg cells was reduced but not to an extent that resulted in dysbiosis and overt clinical colitis in $Itga4^{\Delta DC}$ mice. Our data are in line with the idea that β7 integrins are required for the recruitment of $CD11b^+CD103^+$ DCs to the lamina propria (59) and would support the notion that the α4β7 integrin cooperates with the αEβ7 integrin to guide $CD11b^+CD103^+$ DCs to the lamina propria where these DCs are involved in the induction of pTreg cells. However, long-term observation of $Itga4^{\Delta DC}$ mice will be required to further address this question. Conversely, antigen presentation by $CD11b^+CD103^+$ DCs in the mesenteric lymph node appeared to be intact in $Itga4^{\Delta DC}$ mice because robust *C. rodentium* specific Th17 responses were raised in $Itga4^{\Delta DC}$ mice. Indeed,

$CD11b^+CD103^+$ DCs in the mesenteric lymph nodes were proposed to be the non-redundant source of IL-23 in response to *C. rodentium* derived flagellin to induce IL-22 in ILCs (60) and to prime Th17 responses (58). In steady state, $CD11b^+CD103^+$ DCs had a disadvantage in populating the small intestinal and colonic lamina propria as compared to their α4 integrin sufficient competitors. However, in inflammation (both upon anti-CD3 injection and in *C. rodentium* infection), the recruitment of DCs into the lamina propria and their trafficking to the mesenteric lymph nodes were not obviously impaired in $Itga4^{\Delta DC}$ mice. Although $Itga4^{\Delta DC}$ mice were able to clear a primary *C. rodentium* infection, it is possible that the relative reduction of $CD11b^+CD103^+$ DCs in the lamina propria of $Itga4^{\Delta DC}$ mice affected the generation of *C. rodentium* specific memory T cells with potential consequences for recall responses. Further studies are required to investigate this question in detail.

In conclusion, in this study we definitively show that DC recruitment in the CNS occurs independently of α4 integrin expression both in tissue homeostasis and under inflammatory conditions. Although the DC population in the lamina propria is perturbed in $Itga4^{\Delta DC}$ mice, functional consequences for autoimmunity or host defense do not emanate from this altered DC compartment. Our study illustrates that targeting α4 integrins may not be an efficient means in modulating local APC compartments in the gut and CNS. In particular in the CNS, the tissue specific APC competence is believed to correlate with compartmentalized inflammatory processes during the progressive phase of autoimmune neuroinflammation (in multiple sclerosis) and has been identified as a potential therapeutic target to control tissue restricted chronic inflammation. However, we now provide evidence that other targets than α4 integrins might be more appropriate in re-setting the APC competence of non-lymphoid tissues during prolonged inflammation.

Acknowledgments

We would like to thank Veronika Husterer and Svenja Bourry for their skillful technical assistance.

Author contributions

CS performed most experiments, analyzed data and interpreted results, LGP and SH performed *C. rodentium* infection experiments and analyzed data, MK and DM analyzed histologic data, MP and CO performed and analyzed some lamina propria stainings, AK designed experiments and interpreted results, TK conceived and initiated the study, interpreted results, and wrote the paper.

Conflict of interest

The authors declare that they have no conflict of interest.

References

1. Prodinger, C., J. Bunse, M. Krüger, F. Schiefenhövel, C. Brandt, J. D. Laman, M. Greter, K. Immig, F. Heppner, B. Becher, and I. Bechmann. 2011. CD11c-expressing cells reside in the juxtavascular parenchyma and extend processes into the glia limitans of the mouse nervous system. *Acta Neuropathol* 121: 445–458.

2. Bulloch, K., M. M. Miller, J. Gal-Toth, T. A. Milner, A. Gottfried-Blackmore, E. M. Waters, U. W. Kaunzner, K. Liu, R. Lindquist, M. C. Nussenzweig, R. M. Steinman, and B. S. Mcewen. 2008. CD11c/EYFP transgene illuminates a discrete network of dendritic cells within the embryonic, neonatal, adult, and injured mouse brain. *J. Comp. Neurol.* 508: 687–710.

3. Hickey, W. F., and H. Kimura. 1988. Perivascular microglial cells of the CNS are bone marrow-derived and present antigen in vivo. *Science (New York, NY)* 239: 290–292.

4. Kierdorf, K., D. Erny, T. Goldmann, V. Sander, C. Schulz, E. G. Perdiguero, P. Wieghofer, A. Heinrich, P. Riemke, C. Hölscher, D. N. Muller, B. Luckow, T. Brocker, K. Debowski, G. Fritz, G. Opdenakker, A. Diefenbach, K. Biber, M. Heikenwalder, F. Geissmann, F. Rosenbauer, and M. R. Prinz. 2013. Microglia emerge from erythromyeloid precursors via Pu.1- and Irf8-dependent pathways. *Nat Neurosci* 16: 273–280.

5. Ginhoux, F., M. Greter, M. Leboeuf, S. Nandi, P. See, S. Gokhan, M. F. Mehler, S. J. Conway, L. G. Ng, E. R. Stanley, I. M. Samokhvalov, and M. Merad. 2010. Fate mapping analysis reveals that adult microglia derive from primitive macrophages. *Science (New York, NY)* 330: 841–845.

6. Schulz, C., E. Gomez Perdiguero, L. Chorro, H. Szabo-Rogers, N. Cagnard, K. Kierdorf, M. R. Prinz, B. Wu, S. E. W. Jacobsen, J. W. Pollard, J. Frampton, K. J. Liu, and F. Geissmann. 2012. A lineage of myeloid cells independent of Myb and hematopoietic stem cells. *Science (New York, NY)* 336: 86–90.

7. Greter, M., F. L. Heppner, M. P. Lemos, B. M. Odermatt, N. Goebels, T. Laufer, R. J. Noelle, and B. Becher. 2005. Dendritic cells permit immune invasion of the CNS in an animal model of multiple sclerosis. *Nat Med* 11: 328–334.

8. Immig, K., M. Gericke, F. Menzel, F. Merz, M. Krueger, F. Schiefenhövel, A. Lösche, K. Jäger, U.-K. Hanisch, K. Biber, and I. Bechmann. 2015. CD11c-positive cells from brain, spleen, lung, and liver exhibit site-specific immune phenotypes and plastically adapt to new environments. *Glia* 63: 611–625.

9. Mundt, S., D. Mrdjen, S. G. Utz, M. Greter, B. Schreiner, and B. Becher. 2019. Conventional DCs sample and present myelin antigens in the healthy CNS and allow parenchymal T cell entry to initiate neuroinflammation. *Science immunology* 4: eaau8380.

10. Jordão, M. J. C., R. Sankowski, S. M. Brendecke, Sagar, G. Locatelli, Y.-H. Tai, T. L. Tay, E. Schramm, S. Armbruster, N. Hagemeyer, O. Gross, D. Mai, Ö. Çiçek, T. Falk, M.

Kerschensteiner, D. Grün, and M. R. Prinz. 2019. Single-cell profiling identifies myeloid cell subsets with distinct fates during neuroinflammation. *Science (New York, NY)* 363.

11. Goldmann, T., P. Wieghofer, M. J. C. Jordão, F. Prutek, N. Hagemeyer, K. Frenzel, L. Amann, O. Staszewski, K. Kierdorf, M. Krueger, G. Locatelli, H. Hochgerner, R. Zeiser, S. Epelman, F. Geissmann, J. Priller, F. M. V. Rossi, I. Bechmann, M. Kerschensteiner, S. Linnarsson, S. Jung, and M. R. Prinz. 2016. Origin, fate and dynamics of macrophages at central nervous system interfaces. *Nat Immunol* 17: 797–805.

12. Mrdjen, D., A. Pavlovic, F. J. Hartmann, B. Schreiner, S. G. Utz, B. P. Leung, I. Lelios, F. L. Heppner, J. Kipnis, D. Merkler, M. Greter, and B. Becher. 2018. High-Dimensional Single-Cell Mapping of Central Nervous System Immune Cells Reveals Distinct Myeloid Subsets in Health, Aging, and Disease. 48: 380–395.e6.

13. Jain, P., C. Coisne, G. Enzmann, R. Rottapel, and B. Engelhardt. 2010. Alpha4beta1 integrin mediates the recruitment of immature dendritic cells across the blood-brain barrier during experimental autoimmune encephalomyelitis. *J Immunol* 184: 7196–7206.

14. John, B., B. Ricart, E. D. Tait Wojno, T. H. Harris, L. M. Randall, D. A. Christian, B. Gregg, D. M. De Almeida, W. Weninger, D. A. Hammer, and C. A. Hunter. 2011. Analysis of behavior and trafficking of dendritic cells within the brain during toxoplasmic encephalitis. *PLoS Pathog* 7: e1002246.

15. Anandasabapathy, N., G. D. Victora, M. Meredith, R. Feder, B. Dong, C. Kluger, K. Yao, M. L. Dustin, M. C. Nussenzweig, R. M. Steinman, and K. Liu. 2011. Flt3L controls the development of radiosensitive dendritic cells in the meninges and choroid plexus of the steady-state mouse brain. *J Exp Med* 208: 1695–1705.

16. Irla, M., N. Küpfer, T. Suter, R. Lissilaa, M. Benkhoucha, J. Skupsky, P. H. Lalive, A. Fontana, W. Reith, and S. Hugues. 2010. MHC class II-restricted antigen presentation by plasmacytoid dendritic cells inhibits T cell-mediated autoimmunity. *J Exp Med* 207: 1891–1905.

17. Duraes, F. V., C. Lippens, K. Steinbach, J. Dubrot, D. Brighouse, N. Bendriss-Vermare, S. Issazadeh-Navikas, D. Merkler, and S. Hugues. 2015. pDC therapy induces recovery from EAE by recruiting endogenous pDC to sites of CNS inflammation. *J Autoimmun* 67: 8–18.

18. Isaksson, M., B. Ardesjö, L. Rönnblom, O. Kämpe, H. Lassmann, M.-L. Eloranta, and A. Lobell. 2009. Plasmacytoid DC promote priming of autoimmune Th17 cells and EAE. *Eur J Immunol* 39: 2925–2935.

19. Sie, C., and T. Korn. 2017. Dendritic cells in central nervous system autoimmunity. *Semin Immunopathol* 39: 99–111.

20. Briseño, C. G., T. L. Murphy, and K. M. Murphy. 2014. Complementary diversification of dendritic cells and innate lymphoid cells. *Curr Opin Immunol* 29: 69–78.

21. Persson, E. K., H. Uronen-Hansson, M. Semmrich, A. Rivollier, K. Hägerbrand, J. Marsal, S. Gudjonsson, U. Håkansson, B. Reizis, K. Kotarsky, and W. W. Agace. 2013. IRF4 transcription-factor-dependent CD103(+)CD11b(+) dendritic cells drive mucosal T helper 17 cell differentiation. 38: 958–969.

22. del Rio, M.-L., J.-I. Rodriguez-Barbosa, E. Kremmer, and R. Förster. 2007. CD103- and CD103+ bronchial lymph node dendritic cells are specialized in presenting and cross-presenting innocuous antigen to CD4+ and CD8+ T cells. *J Immunol* 178: 6861–6866.

23. Bedoui, S., P. G. Whitney, J. Waithman, L. Eidsmo, L. Wakim, I. Caminschi, R. S. Allan, M. Wojtasiak, K. Shortman, F. R. Carbone, A. G. Brooks, and W. R. Heath. 2009. Cross-presentation of viral and self antigens by skin-derived CD103+ dendritic cells. *Nat Immunol* 10: 488–495.

24. Hou, B., A. Benson, L. Kuzmich, A. L. DeFranco, and F. Yarovinsky. 2011. Critical coordination of innate immune defense against Toxoplasma gondii by dendritic cells responding via their Toll-like receptors. *Proc Natl Acad Sci USA* 108: 278–283.

25. del Pilar Martin, M., P. D. Cravens, R. Winger, E. M. Frohman, M. K. Racke, T. N. Eagar, S. S. Zamvil, M. S. Weber, B. Hemmer, N. J. Karandikar, B. K. Kleinschmidt-DeMasters, and O. Stüve. 2008. Decrease in the numbers of dendritic cells and CD4+ T cells in cerebral perivascular spaces due to natalizumab. *Arch Neurol* 65: 1596–1603.

26. Derfuss, T., J. M. Kovarik, L. Kappos, M. Savelieva, R. Chhabra, A. Thakur, Y. Zhang, H. Wiendl, and D. Tomic. 2017. α4-integrin receptor desaturation and disease activity return after natalizumab cessation. *Neurol Neuroimmunol Neuroinflamm* 4: e388.

27. Stüve, O., C. M. Marra, K. R. Jerome, L. Cook, P. D. Cravens, S. Cepok, E. M. Frohman, J. T. Phillips, G. Arendt, B. Hemmer, N. L. Monson, and M. K. Racke. 2006. Immune surveillance in multiple sclerosis patients treated with natalizumab. *Annals of neurology* 59: 743–747.

28. Bettelli, E., M. Pagany, H. L. Weiner, C. Linington, R. A. Sobel, and V. K. Kuchroo. 2003. Myelin oligodendrocyte glycoprotein-specific T cell receptor transgenic mice develop spontaneous autoimmune optic neuritis. *J Exp Med* 197: 1073–1081.

29. Bettelli, E., Y. Carrier, W. Gao, T. Korn, T. B. Strom, M. Oukka, H. L. Weiner, and V. K. Kuchroo. 2006. Reciprocal developmental pathways for the generation of pathogenic effector TH17 and regulatory T cells. *Nature* 441: 235–238.

30. Scott, L. M., G. V. Priestley, and T. Papayannopoulou. 2003. Deletion of alpha4 integrins from adult hematopoietic cells reveals roles in homeostasis, regeneration, and homing. *Mol Cell Biol* 23: 9349–9360.

31. Caton, M. L., M. R. Smith-Raska, and B. Reizis. 2007. Notch-RBP-J signaling controls the homeostasis of CD8- dendritic cells in the spleen. *J Exp Med* 204: 1653–1664.

32. Stranges, P. B., J. Watson, C. J. Cooper, C.-M. Choisy-Rossi, A. C. Stonebraker, R. A. Beighton, H. Hartig, J. P. Sundberg, S. Servick, G. Kaufmann, P. J. Fink, and A. V. Chervonsky. 2007. Elimination of antigen-presenting cells and autoreactive T cells by Fas contributes to prevention of autoimmunity. 26: 629–641.

33. Clausen, B. E., C. Burkhardt, W. Reith, R. Renkawitz, and I. Förster. 1999. Conditional gene targeting in macrophages and granulocytes using LysMcre mice. *Transgenic Res* 8: 265–277.

34. Korn, T., M. Mitsdoerffer, A. L. Croxford, A. Awasthi, P. Vollmar, G. L. Stritesky, M. H. Kaplan, and A. Waisman. 2008. IL-6 controls Th17 immunity in vivo by inhibiting the

conversion of conventional T cells into Foxp3+ regulatory T cells. *Proc Natl Acad Sci USA* 105: 18460–18465.

35. Schlitzer, A., A. F. Heiseke, H. Einwächter, W. Reindl, M. Schiemann, C.-P. Manta, P. See, J. H. Niess, T. Suter, F. Ginhoux, and A. B. Krug. 2012. Tissue-specific differentiation of a circulating CCR9- pDC-like common dendritic cell precursor. *Blood* 119: 6063–6071.

36. Rambaldi, D., S. Pece, and P. P. Di Fiore. 2014. flowFit: a Bioconductor package to estimate proliferation in cell-tracking dye studies. *Bioinformatics* 30: 2060–2065.

37. Abram, C. L., G. L. Roberge, Y. Hu, and C. A. Lowell. 2014. Comparative analysis of the efficiency and specificity of myeloid-Cre deleting strains using ROSA-EYFP reporter mice. *J Immunol Methods* 408: 89–100.

38. Baschant, U., L. Frappart, U. Rauchhaus, L. Bruns, H. M. Reichardt, T. Kamradt, R. Bräuer, and J. P. Tuckermann. 2011. Glucocorticoid therapy of antigen-induced arthritis depends on the dimerized glucocorticoid receptor in T cells. *Proc Natl Acad Sci USA* 108: 19317–19322.

39. Croxford, A. L., M. Lanzinger, F. J. Hartmann, B. Schreiner, F. Mair, P. Pelczar, B. E. Clausen, S. Jung, M. Greter, and B. Becher. 2015. The Cytokine GM-CSF Drives the Inflammatory Signature of CCR2+ Monocytes and Licenses Autoimmunity. 43: 502–514.

40. Welsh, C. T., J. W. Rose, K. E. Hill, and J. J. Townsend. 1993. Augmentation of adoptively transferred experimental allergic encephalomyelitis by administration of a monoclonal antibody specific for LFA-1 alpha. *J Neuroimmunol* 43: 161–167.

41. Rose, J. W., C. T. Welsh, K. E. Hill, M. K. Houtchens, R. S. Fujinami, and J. J. Townsend. 1999. Contrasting effects of anti-adhesion molecule therapy in experimental allergic encephalomyelitis and Theiler's murine encephalomyelitis. *J Neuroimmunol* 97: 110–118.

42. Dugger, K. J., K. R. Zinn, C. Weaver, D. C. Bullard, and S. R. Barnum. 2009. Effector and suppressor roles for LFA-1 during the development of experimental autoimmune encephalomyelitis. *J Neuroimmunol* 206: 22–27.

43. Berlin, C., E. L. Berg, M. J. Briskin, D. P. Andrew, P. J. Kilshaw, B. Holzmann, I. L. Weissman, A. Hamann, and E. C. Butcher. 1993. Alpha 4 beta 7 integrin mediates lymphocyte binding to the mucosal vascular addressin MAdCAM-1. *Cell* 74: 185–195.

44. Ohnmacht, C., J.-H. Park, S. Cording, J. B. Wing, K. Atarashi, Y. Obata, V. Gaboriau-Routhiau, R. Marques, S. Dulauroy, M. Fedoseeva, M. Busslinger, N. Cerf-Bensussan, I. G. Boneca, D. Voehringer, K. Hase, K. Honda, S. Sakaguchi, and G. Eberl. 2015. The microbiota regulates type 2 immunity through RORγt+ T cells. *Science (New York, NY)* 349: 989–993.

45. Esplugues, E., S. Huber, N. Gagliani, A. E. Hauser, T. Town, Y. Y. Wan, W. O'connor, A. Rongvaux, N. Van Rooijen, A. M. Haberman, Y. Iwakura, V. K. Kuchroo, J. K. Kolls, J. A. Bluestone, K. C. Herold, and R. A. Flavell. 2011. Control of TH17 cells occurs in the small intestine. *Nature* 475: 514–518.

46. Atarashi, K., T. Tanoue, M. Ando, N. Kamada, Y. Nagano, S. Narushima, W. Suda, A. Imaoka, H. Setoyama, T. Nagamori, E. Ishikawa, T. Shima, T. Hara, S. Kado, T. Jinnohara, H. Ohno, T. Kondo, K. Toyooka, E. Watanabe, S.-I. Yokoyama, S. Tokoro, H. Mori, Y. Noguchi,

H. Morita, I. I. Ivanov, T. Sugiyama, G. Nuñez, J. G. Camp, M. Hattori, Y. Umesaki, and K. Honda. 2015. Th17 Cell Induction by Adhesion of Microbes to Intestinal Epithelial Cells. *Cell* 163: 367–380.

47. Giles, D. A., P. C. Duncker, N. M. Wilkinson, J. M. Washnock-Schmid, and B. M. Segal. 2018. CNS-resident classical DCs play a critical role in CNS autoimmune disease. *J Clin Invest* 128: 5322–5334.

48. Curtin, J. F., G. D. King, C. Barcia, C. Liu, F. X. Hubert, C. Guillonneau, R. Josien, I. Anegon, P. R. Lowenstein, and M. G. Castro. 2006. Fms-like tyrosine kinase 3 ligand recruits plasmacytoid dendritic cells to the brain. *J Immunol* 176: 3566–3577.

49. Quintana, E., A. Fernández, P. Velasco, B. de Andrés, I. Liste, D. Sancho, M. L. Gaspar, and E. Cano. 2015. DNGR-1(+) dendritic cells are located in meningeal membrane and choroid plexus of the noninjured brain. *Glia* 63: 2231–2248.

50. Ji, Q., L. Castelli, and J. M. Goverman. 2013. MHC class I-restricted myelin epitopes are cross-presented by Tip-DCs that promote determinant spreading to $CD8^+$ T cells. *Nat Immunol* 14: 254–261.

51. Rothhammer, V., S. Heink, F. Petermann, R. Srivastava, M. C. Claussen, B. Hemmer, and T. Korn. 2011. Th17 lymphocytes traffic to the central nervous system independently of α4 integrin expression during EAE. *J Exp Med* 208: 2465–2476.

52. King, I. L., T. L. Dickendesher, and B. M. Segal. 2009. Circulating Ly-6C+ myeloid precursors migrate to the CNS and play a pathogenic role during autoimmune demyelinating disease. *Blood* 113: 3190–3197.

53. Mildner, A., M. Mack, H. Schmidt, W. Bruck, M. Djukic, M. D. Zabel, A. Hille, J. Priller, and M. R. Prinz. 2009. CCR2+Ly-6Chi monocytes are crucial for the effector phase of autoimmunity in the central nervous system. *Brain* 132: 2487–2500.

54. Bauer, M., C. Brakebusch, C. Coisne, M. Sixt, H. Wekerle, B. Engelhardt, and R. Fässler. 2009. Beta1 integrins differentially control extravasation of inflammatory cell subsets into the CNS during autoimmunity. *Proc Natl Acad Sci USA* 106: 1920–1925.

55. Coombes, J. L., K. R. R. Siddiqui, C. V. Arancibia-Cárcamo, J. Hall, C.-M. Sun, Y. Belkaid, and F. M. Powrie. 2007. A functionally specialized population of mucosal CD103+ DCs induces Foxp3+ regulatory T cells via a TGF-beta and retinoic acid-dependent mechanism. *J Exp Med* 204: 1757–1764.

56. Lathrop, S. K., S. M. Bloom, S. M. Rao, K. Nutsch, C.-W. Lio, N. Santacruz, D. A. Peterson, T. S. Stappenbeck, and C.-S. Hsieh. 2011. Peripheral education of the immune system by colonic commensal microbiota. *Nature* 478: 250–254.

57. Barthels, C., A. Ogrinc, V. Steyer, S. Meier, F. Simon, M. Wimmer, A. Blutke, T. Straub, U. Zimber-Strobl, E. Lutgens, P. Marconi, C. Ohnmacht, D. Garzetti, B. Stecher, and T. Brocker. 2017. CD40-signalling abrogates induction of RORγt+Treg cells by intestinal CD103+DCs and causes fatal colitis. *Nature communications* 8: 14715.

58. Satpathy, A. T., C. G. Briseño, J. S. Lee, D. Ng, N. A. Manieri, W. Kc, X. Wu, S. R. Thomas, W.-L. Lee, M. Turkoz, K. G. McDonald, M. M. Meredith, C. Song, C. J. Guidos, R. D. Newberry, W. Ouyang, T. L. Murphy, T. S. Stappenbeck, J. L. Gommerman, M. C. Nussenzweig, M. Colonna, R. Kopan, and K. M. Murphy. 2013. Notch2-dependent classical dendritic cells orchestrate intestinal immunity to attaching-and-effacing bacterial pathogens. *Nat Immunol* 14: 937–948.

59. Villablanca, E. J., J. De Calisto, P. Torregrosa Paredes, B. Cassani, D. D. Nguyen, S. Gabrielsson, and J. R. Mora. 2014. β7 integrins are required to give rise to intestinal mononuclear phagocytes with tolerogenic potential. *Gut* 63: 1431–1440.

60. Kinnebrew, M. A., C. G. Buffie, G. E. Diehl, L. A. Zenewicz, I. Leiner, T. M. Hohl, R. A. Flavell, D. R. Littman, and E. G. Pamer. 2012. Interleukin 23 production by intestinal CD103(+)CD11b(+) dendritic cells in response to bacterial flagellin enhances mucosal innate immune defense. 36: 276–287.

Footnotes

[1] This work was supported by a PhD fellowship from the Boehringer Ingelheim Fonds to CS. CO is supported by the ERC (StgG 716718), by the deutsche Forschungsgemeinschaft (SFB 1371-P07 and within FOR2599) and by an intramural fund of the HelmholtzZentrum Muenchen. TK is supported by the Deutsche Forschungsgemeinschaft (SFB1054-B06 to TK, TRR128 to TK, and SyNergy to TK), the German Ministry of Education and Research (BMBF, T-B in NMO), and by the ERC (CoG 647215 to TK).

[2] Correspondence: Thomas Korn, Klinikum rechts der Isar, Technical University of Munich, Ismaninger Str. 22, 81675 Munich, Germany; Phone: ++49-89-41405617; Fax: ++49-89-41404675; E-mail: thomas.korn@tum.de

Figure legends

Figure 1 | DCs accumulate the naive CNS independently of α4 integrin expression.

(A) Immunofluorescence analysis of brain sections from CD11c-GFP expressing *Itga4*$^{\Delta DC(GFP)}$ mice and *Itga4*$^{flox/WT\ DC(GFP)}$ control littermates. Representative tiles showing choroid plexus and meninges. Scale bar, 20 μm.

(B) Flow cytometry analysis of the uninflamed total CNS DC compartment from *Itga4*$^{\Delta DC}$ and *Itga4*$^{flox/flox}$ littermates. Numbers adjacent to gates indicate parent frequency, overall frequency refers to live CD45^{high} cells. Representative pair of 5 mice per genotype. Intravascular cells were excluded from analysis by i.v. application of a CD45 staining antibody prior to dissection. MG, Microglia (CD45^{int}CD11b^{+}), pDC, plasmacytoid dendritic cells (BST-2^{+}CD11b^{-}CD11c^{+}MHC-II^{+}), cDC1 (CD103^{+}CD11b^{low}) and cDC2 (CD103^{-}CD11b^{high}) classical dendritic cells (BST-2^{-}CD11c^{+}MHC-II^{+}).

(C, D) Chimerism between CD45.2 *Itga4*$^{\Delta DC}$ and CD45.1 *Itga4*$^{WT/WT}$ myeloid cells (CD45^{high}) in the uninflamed spleen and CNS of mixed bone-marrow chimeras 8 weeks after reconstitution (mean ± SEM). Gra, Granulocytes (Ly6G^{+}CD11b^{+}B220^{-}CD11c^{-}), Mono, Monocytes (MHCII^{-}CD11c^{-}CD11b^{+}Ly6G^{-}), pDC, plasmacytoid dendritic cells (MHC-II^{+}Siglec-H^{+}BST-2^{+}B220^{+}CD11c^{+}), cDCs, classical dendritic cells (MHC-II^{+}CD11c^{+}Siglec-H^{-}BST-2^{-}B220^{-}) as cDC1 (CD103^{+}CD11b^{low}) and cDC2 (CD103^{-}CD11b^{high}). (C) Chimerism in untreated mice, pooled data from 4 independent experiments. (D) Chimerism 7 days after subcutaneous injection of 5 x 10^{6} Flt3L-secreting B16 melanoma cells, pooled data from 2 independent experiments.

Difference to the reference population (Gra, Granulocytes) was assessed using Dunnett's multiple comparisons test after one-way ANOVA.

Figure 2 | α4 integrins on DC are dispensable for active induction of EAE.

(A) EAE disease course in *Itga4*$^{\Delta DC}$, *Itga4*$^{\Delta DC\Delta Mo}$ and *Itga4*$^{flox/flox}$ control littermates after active immunization with MOG(35–55) in CFA and intravenous PTX administration (mean ± SEM). Pooled data from four independent experiments. Groups were statistically compared on a per-day basis using a one-way ANOVA followed by Dunnett's multiple comparison test.

(B) Gating strategy and *Itga4* ablation efficiency in myeloid cells of the CNS as measured by flow cytometry at peak disease of active EAE. MG, Microglia (CD45^{int}CD11b^{+}), pDC (MHC-II^{+} CD11c^{+}BST-2^{+}CD11b^{-}), cDC1 (MHCII^{+}CD11c^{+}BST-2^{-}CD64^{-}CD11b^{int}CD103^{+}), moDC, Monocyte-derived dendritic cells (MHC-II^{+}CD64^{+}CD11b^{+}).

(C) Relative fraction and absolute number of myeloid cells in spinal cords of *Itga4*$^{\Delta DC}$ mice, *Itga4*$^{\Delta DC\Delta Mo}$ mice, and *Itga4*$^{flox/flox}$ control littermates at EAE peak disease as measured by flow cytometry (mean ± SEM). Representative example from 4 independent experiments with a total number of at least 10 mice per genotype. Groups were statistically compared using a two-way ANOVA followed by Sidak's multiple comparisons test.

(D, E) Chimerism between CD45.2 *Itga4*$^{\Delta DC}$ (D) or CD45.2 *Itga4*$^{\Delta DC\Delta Mo}$ (E) and CD45.1 Itga4$^{WT/WT}$ myeloid cells in the indicated organs of mixed bone-marrow chimeric EAE mice at peak disease (mean ± SEM). Pooled data from four independent experiments. Statistically significant differences in comparison to the control population Gra, Granulocytes (MHC-II^{-} CD11b^{+}CD64^{-}CD11c^{-}BST-2^{-}Ly6C^{+}Ly6G^{+}) are reported for each organ according to Dunnett's

multiple comparison post-hoc test following overall significant difference in one-way ANOVA (Multiplicity adjusted p-values: **p<0.01; ***p<0.001).

Figure 3 | *Itga4*$^{\Delta DC}$ mice are fully competent in restimulating encephalitogenic T cells within the CNS compartment.

(A) Disease course in *Itga4*$^{\Delta DC}$ mice, *Itga4*$^{\Delta DC\Delta Mo}$ mice, and *Itga4*$^{flox/flox}$ littermate control mice following intravenous transfer of 5 x 10^6 MACS-enriched, $CD4^+$ T cells that had been cultured for 3 days under Th17 skewing conditions (TGF-β, IL-6, IL-23) in the presence of MOG(35–55) and isolated from wild-type donors 7 days after immunization with MOG(35–55) in CFA. Pooled data from three independent experiments (mean ± SEM). Groups were statistically compared on a per-day basis using a one-way ANOVA followed by Dunnett's multiple comparison test.

(B) Relative fraction and absolute number of myeloid cells in the spinal cord of *Itga4*$^{\Delta DC}$, *Itga4*$^{\Delta DC\Delta Mo}$ and *Itga4*$^{flox/flox}$ recipients of encephalitogenic T cells at AT-EAE peak disease as measured by flow cytometry (mean ± SEM). pDC ($BST\text{-}2^+CD11b^-CD11c^+$), cDC1 ($BST\text{-}2^-CD11c^+CD11b^{int}CD103^+$), moDC ($CD64^+CD11b^+$). Pooled data from five independent experiments. Groups were statistically compared using a two-way ANOVA followed by Sidak's multiple comparisons test.

Figure 4 | Steady state accumulation of CD11b^{+}CD103^{+} DCs in the gut lamina propria is dependent on α4 integrin expression.

(A) Relative fractions and ratio of CD11b^{+} and CD11b^{-} subsets of the CD103^{+} DC population (MHC-II^{+}CD64^{-}CD11c^{+}CD103^{+}) in small intestine (SI), colon (Col) and mesenteric lymph nodes (mLN) of naive *Itga4*$^{\Delta DC}$ mice and *Itga4*$^{flox/flox}$ littermate controls as determined by flow cytometry (mean ± SEM). Connecting lines indicate sex-matched, co-housed littermates analyzed on the same day. Pooled data from at least 5 independent experiments shown. Statistical significance reported from paired two-tailed t tests (*p<0.05; **p<0.01; ***p<0.001).

(B) Chimerism between CD45.2 *Itga4*$^{\Delta DC}$ (KO) and CD45.1 *Itga4*$^{WT/WT}$ (WT) myeloid cells in the indicated organs of naive mixed bone-marrow chimeric mice (mean ± SEM). Pooled data from two independent experiments. Statistically significant differences as compared to the control population Gra, Granulocytes (SSC^{high}Ly6G^{+}CD3e^{-}) are shown for each organ according to Dunnett's multiple comparison post-hoc test following overall significant difference in one-way ANOVA (Multiplicity adjusted p-values: *p<0.05; **p<0.01; ***p<0.001).

Figure 5 | Effector T cell priming and host defense in the gut is not dependent on α4 integrin expression by DCs.

(A) Relative body weight loss of *Itga4*$^{\Delta DC}$ mice and *Itga4*$^{flox/flox}$ littermates following repetitive intraperitoneal injection of 20 µg anti-CD3 antibody as indicated. Groups were compared statistically using two-way ANOVA followed by Sidak's multiple comparisons test. Representative experiment with at least 10 mice per genotype shown (mean ± SEM).

(B) Survival curve of *Itga4*$^{\Delta DC}$ mice and *Itga4*$^{flox/flox}$ littermate control mice infected with *Citrobacter rodentium*. Groups were statistically compared using a Log-rank (Mantel-Cox) test.

(C) Bacterial load in feces derived from colon and caecum of *Citrobacter*-infected *Itga4*$^{\Delta DC}$ mice and *Itga4*$^{flox/flox}$ littermates on day 7 after infection (mean ± SEM). Groups were statistically compared using a two-tailed, unpaired Student's t test.

(D) Relative fraction of myeloid cells in the colon and mesenteric lymph nodes of *Itga4*$^{\Delta DC}$ mice and *Itga4*$^{flox/flox}$ littermate control mice infected with *Citrobacter rodentium* as analyzed by flow cytometry 7 days after infection (mean ± SEM). Groups were compared using a one-way ANOVA followed by Sidak's multiple comparisons test.

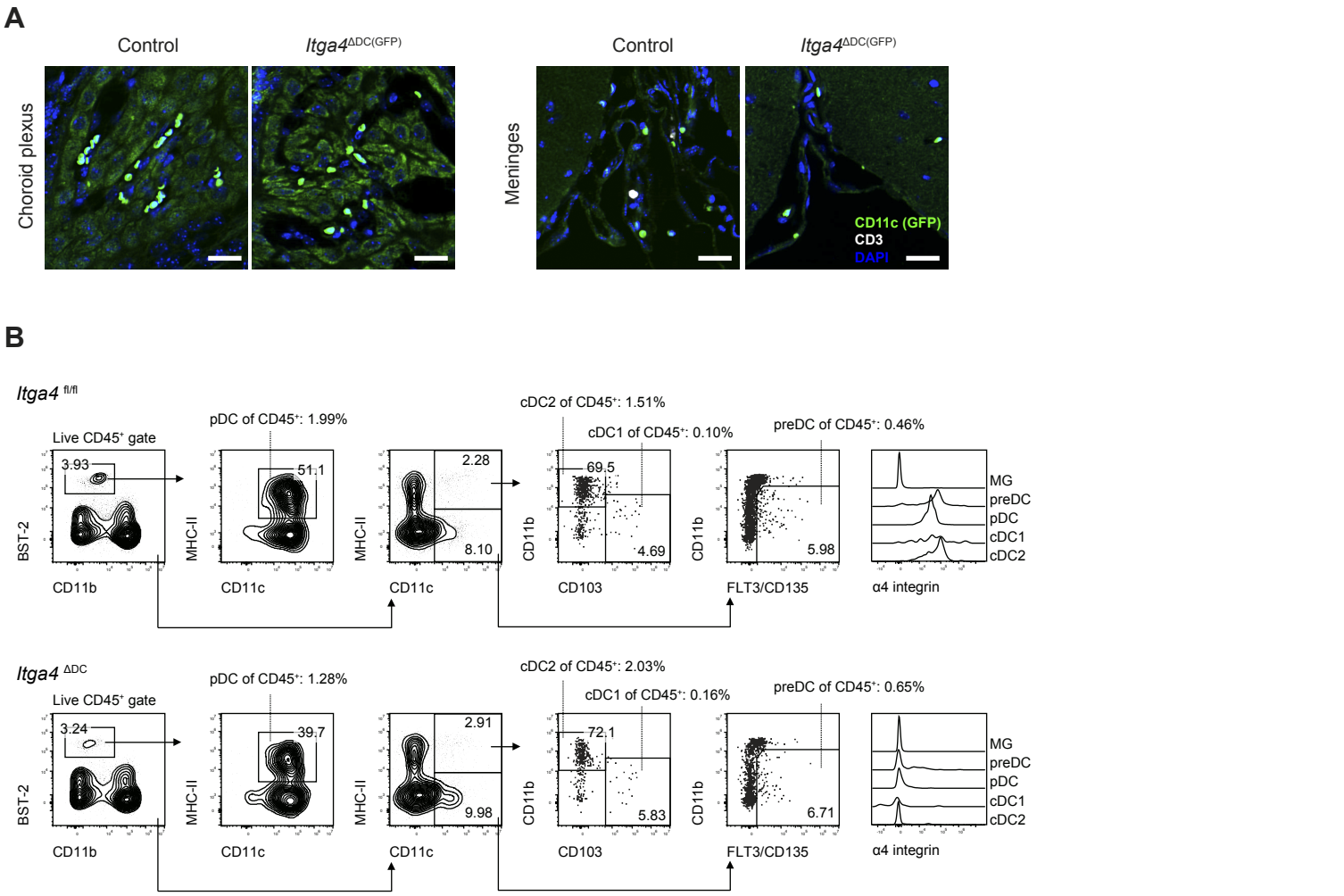
A
Control
Itga4ΔDC(GFP)
Control
Itga4ΔDC(GFP)
Choroid plexus
Meninges
CD11c (GFP)
CD3
DAPI
B
Itga4 fl/fl
Live CD45+ gate
pDC of CD45+: 1.99%
cDC2 of CD45+: 1.51%
cDC1 of CD45+: 0.10%
preDC of CD45+: 0.46%
3.93
51.1
2.28
8.10
69.5
4.69
5.98
BST-2
MHC-II
CD11b
CD11c
CD103
FLT3/CD135
α4 integrin
MG
preDC
pDC
cDC1
cDC2
Itga4 ΔDC
Live CD45+ gate
pDC of CD45+: 1.28%
cDC2 of CD45+: 2.03%
cDC1 of CD45+: 0.16%
preDC of CD45+: 0.65%
3.24
39.7
2.91
9.98
72.1
5.83
6.71
C
SPL
CNS
Percent of subset
CD45.2 KO
CD45.1 WT
Gra
Mono
pDC
cDC1
cDC2
D
SPL (Flt3L)
CNS (Flt3L)

Figure 2

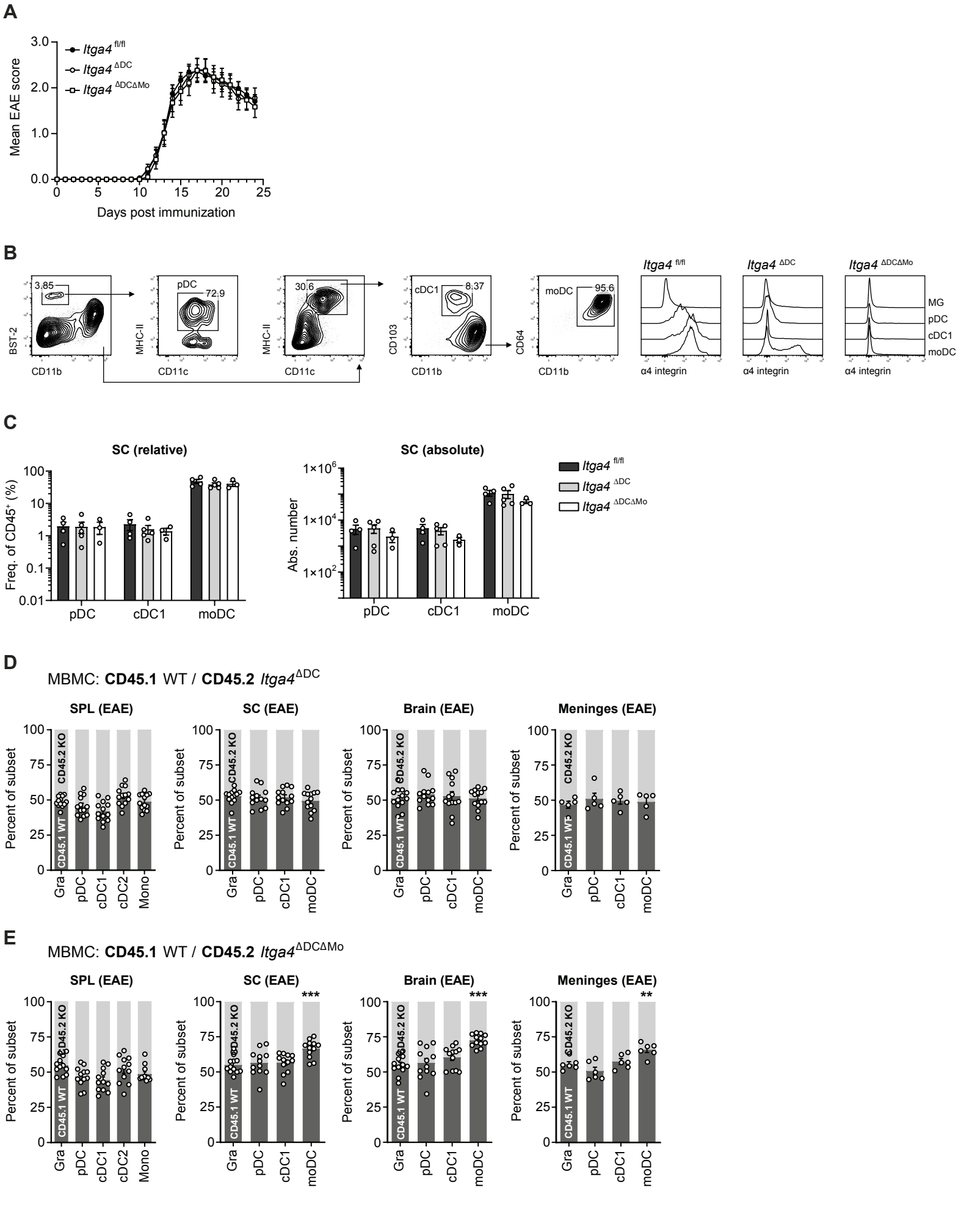
A
Mean EAE score
Days post immunization
Itga4 fl/fl
Itga4 ΔDC
Itga4 ΔDCΔMo
B
BST-2
CD11b
pDC
MHC-II
CD11c
cDC1
CD103
moDC
CD64
α4 integrin
MG
C
SC (relative)
SC (absolute)
Freq. of CD45+ (%)
Abs. number
pDC
cDC1
moDC
D
MBMC: CD45.1 WT / CD45.2 Itga4ΔDC
SPL (EAE)
SC (EAE)
Brain (EAE)
Meninges (EAE)
Percent of subset
CD45.1 WT
CD45.2 KO
Gra
pDC
cDC1
cDC2
Mono
moDC
E
MBMC: CD45.1 WT / CD45.2 Itga4ΔDCΔMo
***
**

Figure 3

A

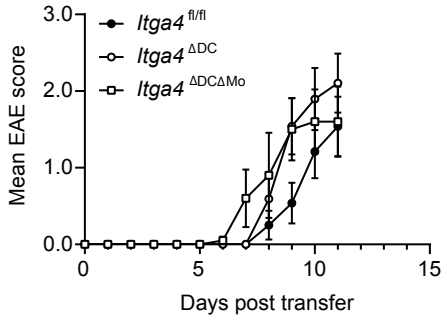
3.0
2.0
1.0
0.0
Mean EAE score
0
5
10
15
Days post transfer
Itga4 fl/fl
Itga4 ΔDC
Itga4 ΔDCΔMo

B

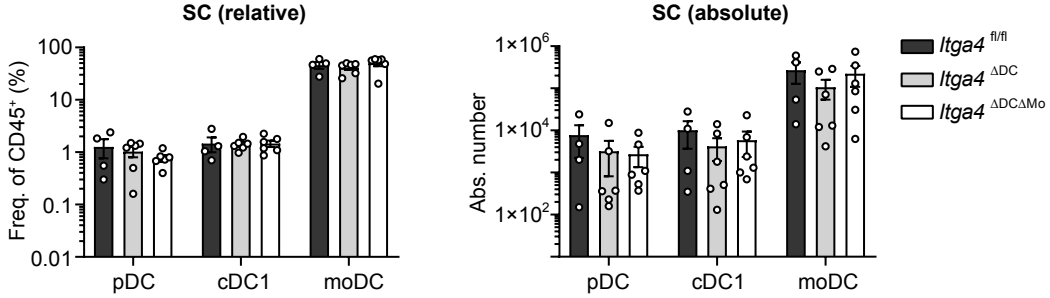
SC (relative)
Freq. of CD45+ (%)
100
10
1
0.1
0.01
pDC
cDC1
moDC
SC (absolute)
Abs. number
1×10^6
1×10^4
1×10^2
pDC
cDC1
moDC
Itga4 fl/fl
Itga4 ΔDC
Itga4 ΔDCΔMo

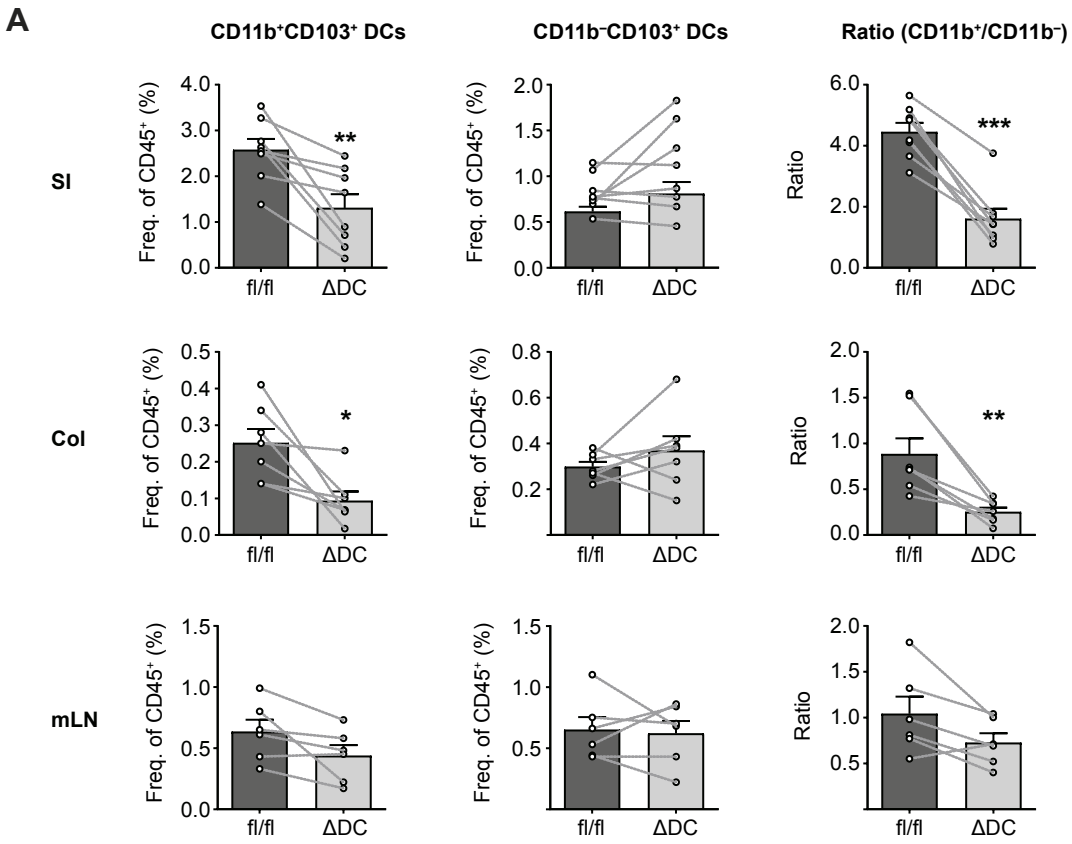
A
CD11b+CD103+ DCs
CD11b−CD103+ DCs
Ratio (CD11b+/CD11b−)
SI
Col
mLN
Freq. of CD45+ (%)
Ratio
fl/fl
ΔDC
**
*
***

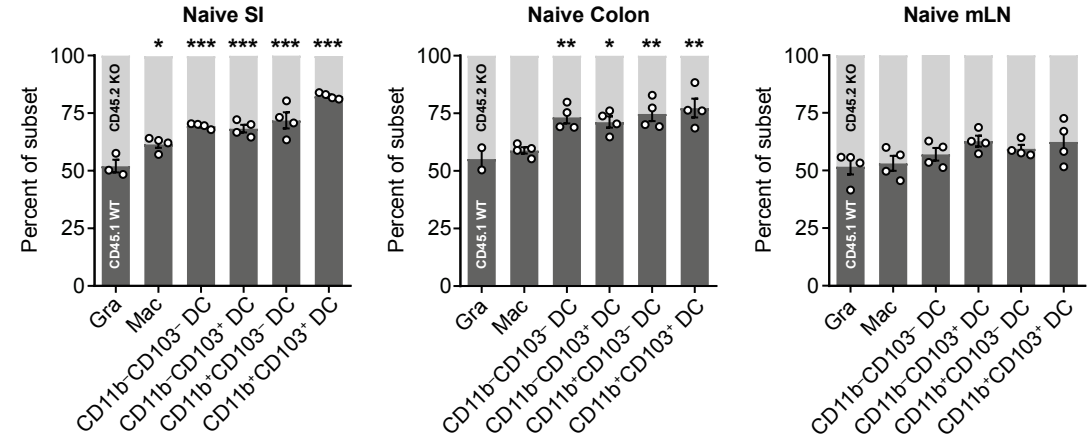
B
MBMC: CD45.1 WT / CD45.2 Itga4ΔDC
Naive SI
Naive Colon
Naive mLN
Percent of subset
CD45.1 WT
CD45.2 KO
Gra
Mac
CD11b−CD103− DC
CD11b−CD103+ DC
CD11b+CD103− DC
CD11b+CD103+ DC

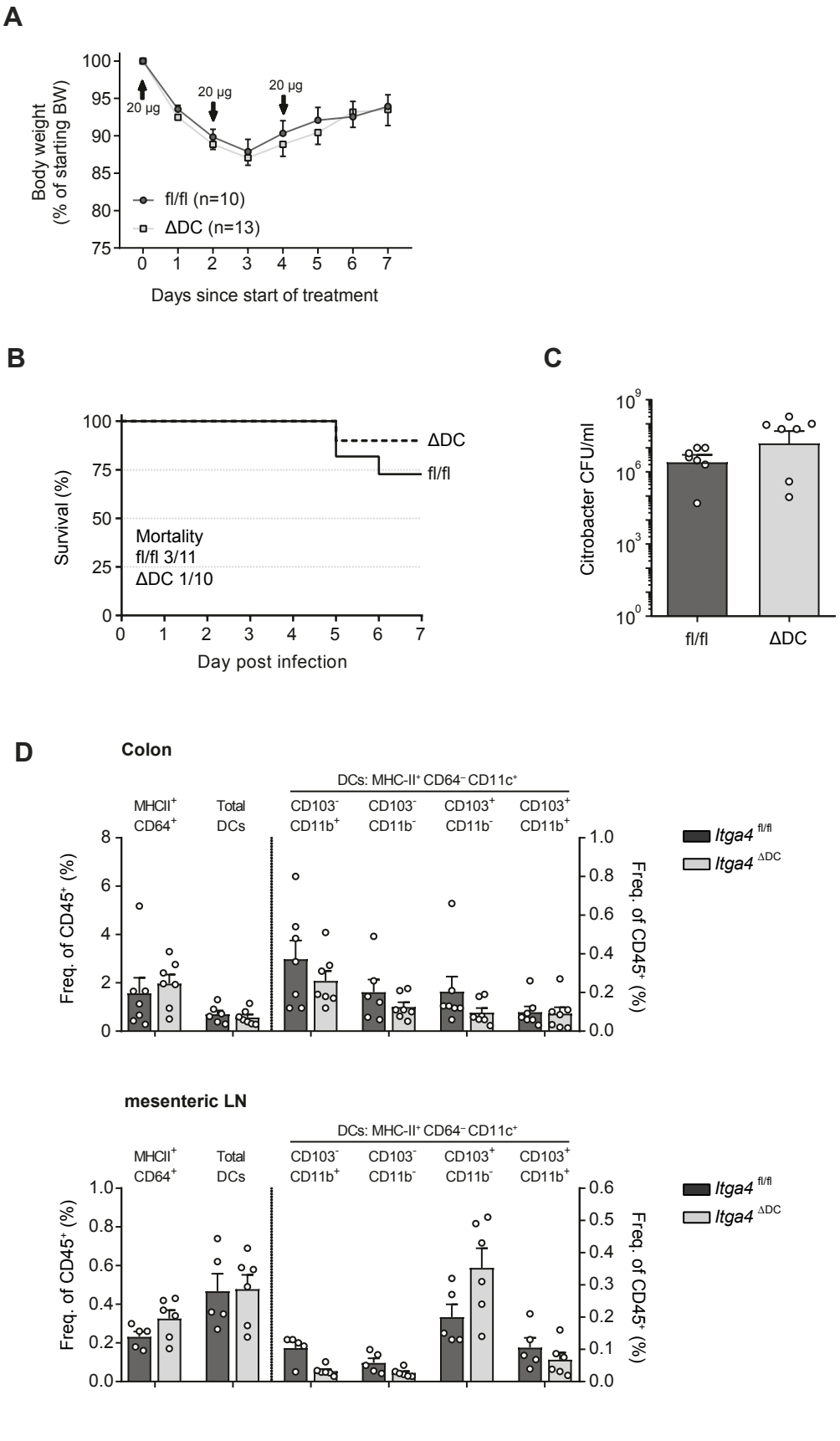
A
Body weight (% of starting BW)
20 µg
20 µg
20 µg
fl/fl (n=10)
ΔDC (n=13)
Days since start of treatment
B
Survival (%)
ΔDC
fl/fl
Mortality
fl/fl 3/11
ΔDC 1/10
Day post infection
C
Citrobacter CFU/ml
fl/fl
ΔDC
D
Colon
DCs: MHC-II+ CD64- CD11c+
MHCII+ CD64+
Total DCs
CD103- CD11b+
CD103- CD11b-
CD103+ CD11b-
CD103+ CD11b+
Freq. of CD45+ (%)
Itga4 fl/fl
Itga4 ΔDC
mesenteric LN

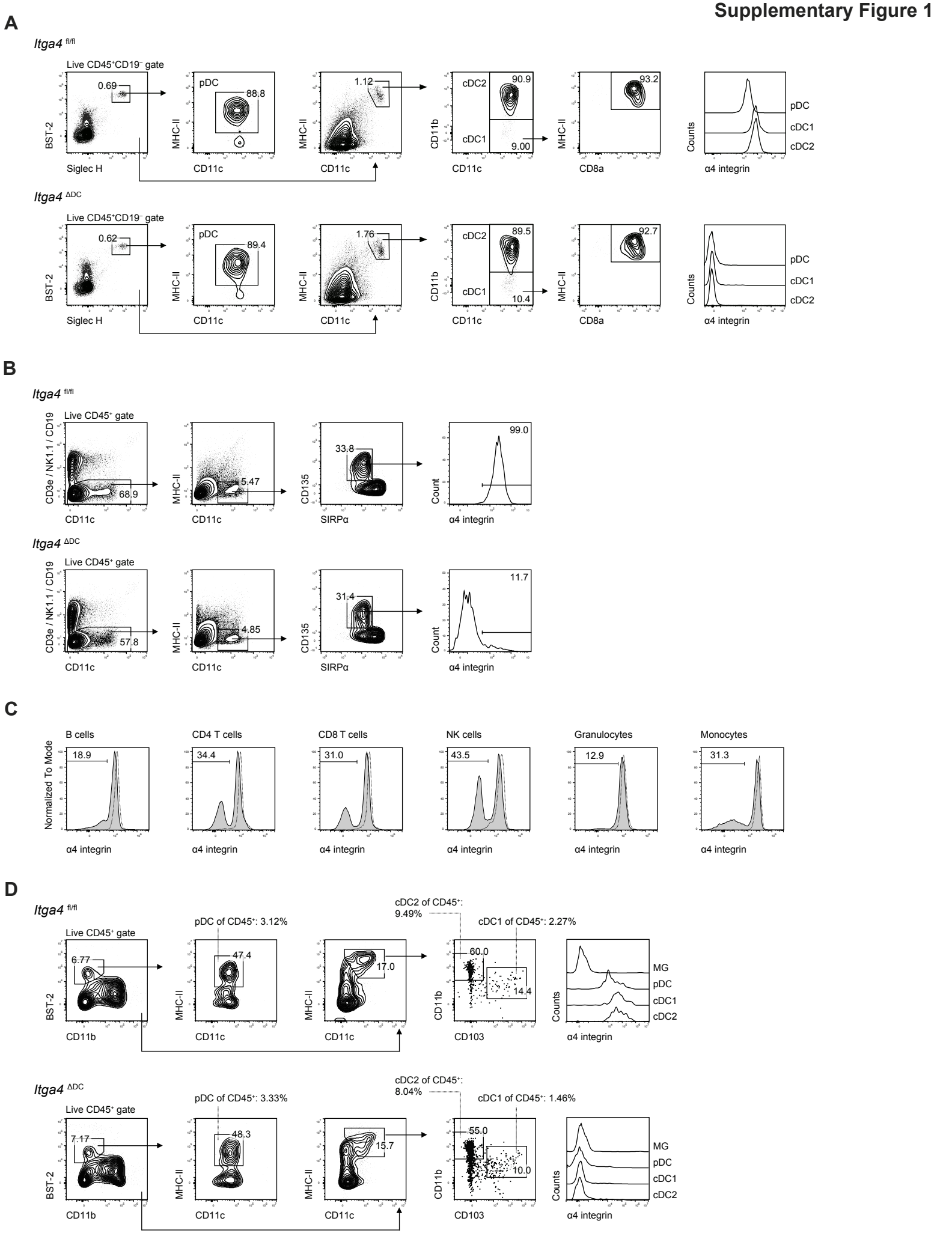
A
Itga4 fl/fl
Live CD45+CD19− gate
0.69
BST-2
Siglec H
pDC
88.8
MHC-II
CD11c
1.12
MHC-II
CD11c
cDC2
90.9
cDC1
9.00
CD11b
CD11c
93.2
MHC-II
CD8a
pDC
cDC1
cDC2
Counts
α4 integrin
Itga4 ΔDC
Live CD45+CD19− gate
0.62
BST-2
Siglec H
pDC
89.4
MHC-II
CD11c
1.76
MHC-II
CD11c
cDC2
89.5
cDC1
10.4
CD11b
CD11c
92.7
MHC-II
CD8a
pDC
cDC1
cDC2
Counts
α4 integrin
B
Itga4 fl/fl
Live CD45+ gate
CD3e / NK1.1 / CD19
68.9
CD11c
MHC-II
5.47
CD11c
CD135
33.8
SIRPα
Count
99.0
α4 integrin
Itga4 ΔDC
Live CD45+ gate
CD3e / NK1.1 / CD19
57.8
CD11c
MHC-II
4.85
CD11c
CD135
31.4
SIRPα
Count
11.7
α4 integrin
C
B cells
18.9
CD4 T cells
34.4
CD8 T cells
31.0
NK cells
43.5
Granulocytes
12.9
Monocytes
31.3
Normalized To Mode
α4 integrin
D
Itga4 fl/fl
Live CD45+ gate
6.77
BST-2
CD11b
pDC of CD45+: 3.12%
47.4
MHC-II
CD11c
17.0
MHC-II
CD11c
cDC2 of CD45+: 9.49%
cDC1 of CD45+: 2.27%
60.0
14.4
CD11b
CD103
MG
pDC
cDC1
cDC2
Counts
α4 integrin
Itga4 ΔDC
Live CD45+ gate
7.17
BST-2
CD11b
pDC of CD45+: 3.33%
48.3
MHC-II
CD11c
15.7
MHC-II
CD11c
cDC2 of CD45+: 8.04%
cDC1 of CD45+: 1.46%
55.0
10.0
CD11b
CD103
MG
pDC
cDC1
cDC2
Counts
α4 integrin

Supplementary Figure 1 | Efficiency of *Itga4* ablation in spleen, bone marrow and Flt3L-treated CNS.

(A) Efficiency of ablation in the spleen. Dendritic cells from naive spleens of *Itga4*$^{\Delta DC}$ mice and *Itga4*$^{flox/flox}$ control mice were isolated and analyzed by flow cytometry. pDC (CD19$^-$MHC-II$^+$Siglec-H$^+$BST-2$^+$CD11c$^+$), cDC1 (CD19$^-$MHC-II$^+$Siglec-H$^-$BST-2$^-$CD11c$^+$ CD11b$^-$) and cDC2 (CD19$^-$MHC-II$^+$Siglec H$^-$BST-2$^-$CD11c$^+$CD11b$^+$). Representative plot of 5 mice per genotype.

(B) DC progenitors already exhibit an extensive loss of surface α4 integrin expression in the bone marrow of *Itga4*$^{\Delta DC}$ mice. Pre-cDCs (CD45$^+$CD3e$^-$NK1.1$^-$CD19$^-$MHC-II$^-$CD11c$^+$CD135$^+$CD172a^{int}) were isolated from the femoral bone marrow of naive *Itga4*$^{\Delta DC}$ mice and *Itga4*$^{flox/flox}$ littermates and analyzed for α4 integrin expression by flow cytometry. Representative plot of 5 mice per genotype.

(C) Specificity of *Itga4* ablation in the spleen. Splenocytes from *Itga4*$^{\Delta DC}$ mice (shaded histograms) and *Itga4*$^{flox/flox}$ (overlaid dotted lines) were isolated and analyzed by flow cytometry. B cells (CD19$^+$B220$^+$MHC-II$^+$CD3e$^-$CD11b$^-$), CD4 T cells (CD3e$^+$CD19$^-$MHC-II$^-$CD11b$^-$CD4$^+$ CD8$^-$), CD8 T cells (CD3e$^+$CD19$^-$MHC$^-$CD11b$^-$CD4$^-$CD8$^+$), NK cells (MHC-II$^-$CD11b$^-$CD3e$^-$NK1.1$^+$), Granulocytes (Ly6G$^+$Ly6C$^+$SSC^{high}) and Monocytes (Ly6G$^-$CD19$^-$CD11b$^+$ F4/80$^+$ Ly6C$^+$). Number above gate indicates fraction of α4 integrin negative cells for the respective leukocyte type in *Itga4*$^{\Delta DC}$ mice, given in percent. Representative plots of 5 mice per genotype.

(D) Flow cytometric analysis of the uninflamed total CNS DC compartment from *Itga4*$^{\Delta DC}$ mice and *Itga4*$^{flox/flox}$ littermates 7 days after subcutaneous injection of 5x10^6 Flt3L-secreting B16 melanoma cells. Numbers adjacent to gates indicate parent frequency, overall frequency refers to live CD45^{high} cells. Representative pair of 5 mice per genotype. Intravascular cells were excluded from analysis by i.v. application of a CD45 staining antibody prior to dissection. MG, Microglia (CD45^{int}CD11b$^+$), pDC (BST-2$^+$CD11b$^-$CD11c$^+$MHC-II$^+$), cDC1 (CD103$^+$CD11b^{low}) and cDC2 (CD103$^-$CD11b^{high}) classical dendritic cells (BST-2$^-$CD11c$^+$MHC-II$^+$).

Supplementary Figure 2

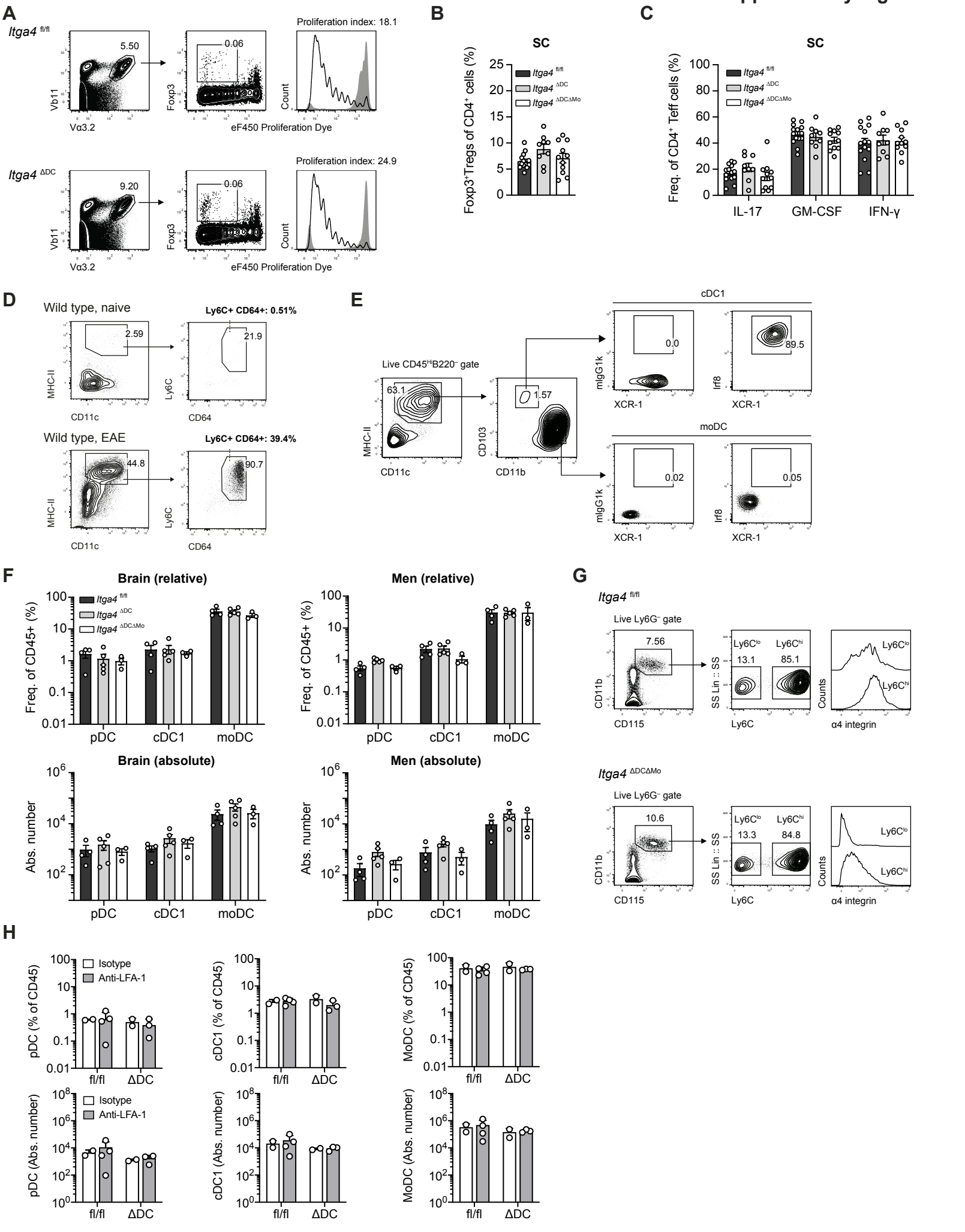

Supplementary Figure 2 | T cell responses are not altered in mice harboring α4 integrin-deficient DCs during active EAE.

(A) The *Itga4*$^{\Delta DC}$ APC compartment can efficiently prime T cell responses in draining lymph nodes after immunization. Naive CD4^{+}Foxp3 (GFP)$^{-}$ T cells were sorted from Foxp3.GFP x 2D2 mice, labeled with eF450 cell proliferation dye and intravenously transferred into *Itga4*$^{\Delta DC}$ and *Itga4*$^{flox/flox}$ control hosts followed by immunization with MOG(35-55) in CFA. After 4 days, T cells were re-isolated from draining lymph nodes. Dilution of proliferation dye and Treg cell induction were assessed by flow cytometry and proliferation index calculated using the flowFit package in R. Representative plot of 3 mice per genotype.

(B) Fraction of Foxp3^{+} Treg cells among CD4^{+} T cells in the spinal cord of mice of the indicated genotype at the peak of EAE. Pooled data from five independent experiments (mean ± SEM). Groups were compared using one-way ANOVA followed by Tukey's multiple comparisons test.

(C) Spinal cord-infiltrating effector T cells exhibit similar cytokine profiles in *Itga4*$^{\Delta DC}$ mice and *Itga4*$^{flox/flox}$ control animals during EAE. Mice were immunized with MOG(35–55) in CFA and PTX. Infiltrating lymphocytes were isolated at peak disease, stimulated for 3h in the presence of PMA, ionomycin and monensin, and assessed for intracellular cytokines by flow cytometry. The reference gate was set at CD4^{+}Foxp3^{-} effector T cells (Teff). Pooled data from five independent experiments (mean ± SEM). Groups were compared using two-way ANOVA followed by Sidak's multiple comparisons test.

(D) MoDCs are a prominent population in the CNS of EAE-diseased, but not healthy mice. Wild type mice were immunized with MOG(35–55) in CFA and PTX. At peak disease, mice were subjected to intravascular staining and perfusion to exclude blood contamination, followed by isolation of CNS mononuclear cells from EAE mice and naive littermates. Gated for CD45high, B220-, extravascular, live cells. Percentages above plots indicate fraction relative to all CD45^{high} live cells.

(E) Intranuclear Irf8 staining with corresponding isotype control (mIgG1k) in cDC1s and moDCs isolated from the CNS of *Itga4*$^{flox/flox}$ control mice at the peak of active EAE.

(F) Relative fraction and absolute number of myeloid cells in the brain and meninges (Men) of *Itga4*$^{\Delta DC}$ mice, *Itga4*$^{\Delta DC\Delta Mo}$ mice, and *Itga4*$^{flox/flox}$ control littermates at EAE peak disease as measured by flow cytometry (mean ± SEM). Representative example from 4 independent experiments with a total number of at least 10 mice per genotype. Groups were statistically compared using a two-way ANOVA followed by Sidak's multiple comparisons test.

(G) *Itga4*$^{\Delta DC\Delta Mo}$ mice and *Itga4*$^{flox/flox}$ control littermates were s.c. immunized with MOG(35-55) in CFA and PTX. On day 7 after immunization, peripheral blood monocytes (CD45^{+}, CD11b^{+}, Ly6G^{-}, CD115^{+}, Ly6C$^{+/-}$) were isolated and analyzed for α4 integrin expression. Representative plot of 5 mice per genotype.

(H) *Itga4*$^{\Delta DC}$ mice and *Itga4*$^{flox/flox}$ control littermates were s.c. immunized with MOG(35-55) in CFA and PTX. Starting on day 5 after immunization, mice were injected i.p. with 200 µg anti-LFA-1 (clone M17/4) or isotype (clone 2A3), followed by injection of 100 µg every other day until day 15. Shortly after, leukocytes were isolated from the brain of mice at peak disease and analyzed by flow cytometry for fractions (top row) and absolute numbers (bottom row, mean ± SEM). Groups were statistically compared using a two-way ANOVA followed by Sidak's multiple comparisons test.

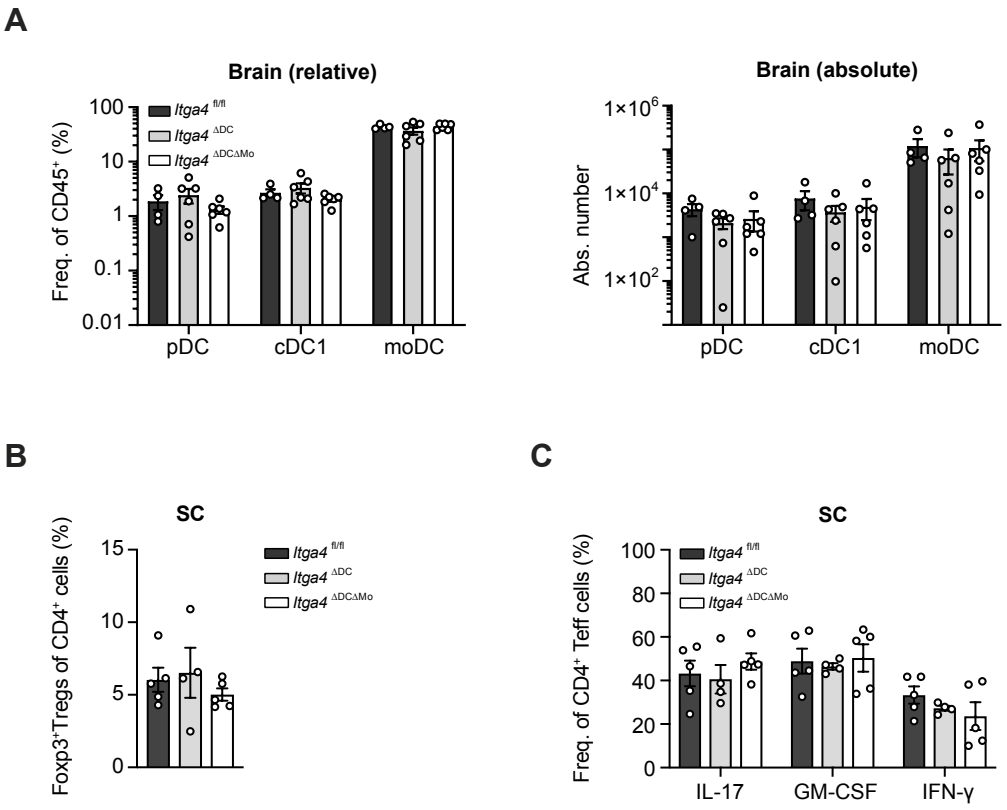

Supplementary Figure 3 | The reactivation of T cells in the CNS is not dependent on α4 integrin expression on DCs during AT-EAE.

(A) Relative fraction and absolute number of myeloid cells in the brain of *Itga4*$^{\Delta DC}$, *Itga4*$^{\Delta DC\Delta Mo}$ and *Itga4*$^{flox/flox}$ recipients of encephalitogenic T cells at AT-EAE peak disease as measured by flow cytometry. pDC (BST-2$^+$ CD11b$^-$CD11c$^+$), cDC1 (CD11c$^+$CD11b^{int}CD103$^+$), MoDC (CD64$^+$CD11b$^+$). Pooled data from five independent experiments (mean ± SEM). Groups were statistically compared using a two-way ANOVA followed by Sidak's multiple comparisons test.

(B) Fraction of Foxp3$^+$ Treg cells among CD4$^+$ T cells in the spinal cord of mice of the indicated genotype at peak disease of adoptive transfer EAE. Pooled data from four independent experiments (mean ± SEM). Groups were compared using one-way ANOVA followed by Tukey's multiple comparisons test.

(C) CNS-infiltrating T cells exhibit similar cytokine profiles in *Itga4*$^{\Delta DC}$ mice and *Itga4*$^{flox/flox}$ control mice in AT-EAE. *Itga4*$^{\Delta DC}$ mice, *Itga4*$^{\Delta DC\Delta Mo}$ mice and *Itga4*$^{flox/flox}$ control littermates were injected with 5x10^6 encephalitogenic T cells and total CNS infiltrating lymphocytes were isolated at peak disease, stimulated for 3h in the presence of PMA, ionomycin and monensin and analyzed in flow cytometry. The reference gate was set at CD4$^+$Foxp3$^-$ effector T cells (Teff). Pooled data from four independent experiments (mean ± SEM). Groups were compared using two-way ANOVA followed by Sidak's multiple comparisons test.

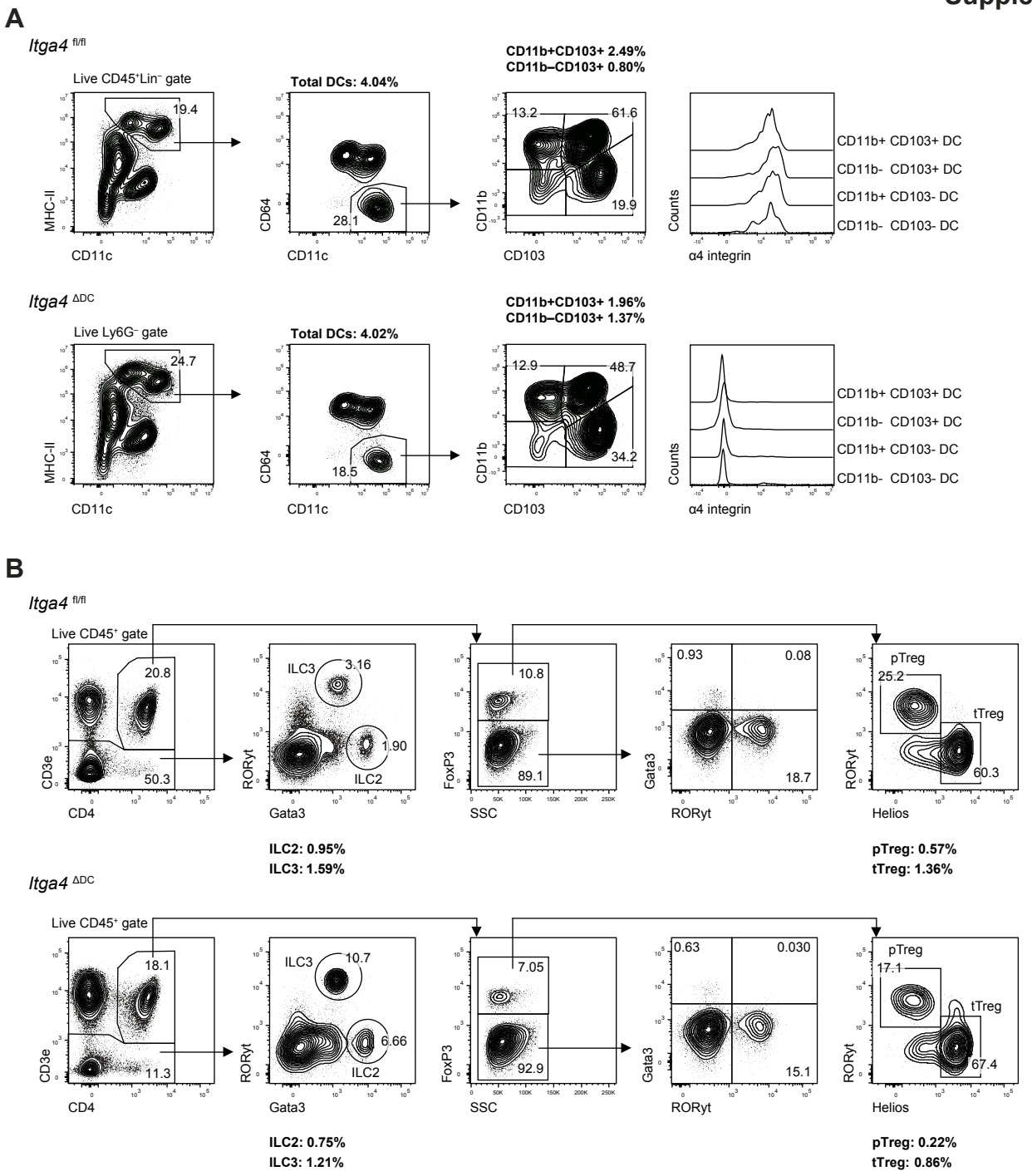

Supplementary Figure 4 | Efficiency of *Itga4* ablation and distribution of ILCs and lamina propria T cells in the intestine of unmanipulated *Itga4*$^{\Delta DC}$ mice.

(A) Small intestinal lamina propria cells were isolated from naive *Itga4*$^{\Delta DC}$ and *Itga4*$^{flox/flox}$ mice and stained for DC subsets according to the indicated gating strategy. The efficiency of α4 integrin ablation in DC subsets is shown according to their CD11b and CD103 status. Fractions adjacent to gates indicate parent frequency, fractions outside of plots refer to all live CD45$^+$ cells.

(B) T cells and ILCs from the small intestinal lamina propria of naive *Itga4*$^{\Delta DC}$ and *Itga4*$^{flox/flox}$ mice were isolated and analyzed by flow cytometry. ILC2, Type 2 innate lymphocyte (CD3$^-$Gata3$^+$RORγt$^-$), ILC3, Type 3 innate lymphocyte (CD3$^-$Gata3$^-$RORγt$^+$), pTreg, peripherally induced regulatory T cells (CD3$^+$CD4$^+$Foxp3$^+$RORγt$^+$ Helios$^-$), tTreg, thymus-derived regulatory T cells (CD3$^+$CD4$^+$Foxp3$^+$RORγt$^-$Helios$^+$). Fractions adjacent to gates indicate parent frequency, fractions outside of plots refer to all live CD45$^+$ cells.